Site U1454

Christian France-Lanord, Volkhard Spiess, Adam Klauss, R.R. Adhikari, S.K. Adhikari, J.-J. Bahk, A.T. Baxter, J.W. Cruz, S.K. Das, P. Dekens, et al.

France-Lanord, C., Spiess, V., Klaus, A., Schwenk, T., and the Expedition 354 Scientists
Proceedings of the International Ocean Discovery Program Volume 354
publications.iodp.org

doi:10.14379/iodp.proc.354.108.2016

Site U1454[1]

C. France-Lanord, V. Spiess, A. Klaus, R.R. Adhikari, S.K. Adhikari, J.-J. Bahk, A.T. Baxter, J.W. Cruz, S.K. Das, P. Dekens, W. Duleba, L.R. Fox, A. Galy, V. Galy, J. Ge, J.D. Gleason, B.R. Gyawali, P. Huyghe, G. Jia, H. Lantzsch, M.C. Manoj, Y. Martos Martin, L. Meynadier, Y.M.R. Najman, A. Nakajima, C. Ponton, B.T. Reilly, K.G. Rogers, J.F. Savian, T. Schwenk, P.A. Selkin, M.E. Weber, T. Williams, and K. Yoshida[2]

Keywords: International Ocean Discovery Program, IODP, Expedition 354, *JOIDES Resolution*, Site U1454, Bengal Fan

Contents

Site summary

Site U1454 (proposed Site MBF-7A) is the westernmost of the transect of seven shallow-penetration sites drilled in the Bengal Fan at 8°N during Expedition 354. The site was introduced during the expedition as an alternate site to capture the most recent and Late Pleistocene fan deposition at high resolution. Expedition 354 sites in the eastern and central part of the transect revealed that fan deposition above and below the Toba ash layer (~75 ka) was remarkably low, indicating migration of turbidite channel activity to the west of the 85°East Ridge for probably the last 300 ky.

Site U1454 is located ~50 km west of Site U1455 (Deep Sea Drilling Project [DSDP] Site 218) at 08°0.39′N, 85°51.00′E, in a water depth of 3721.4 m. It is situated on the western levee of a channel-levee system believed to be the modern active channel of the fan (Hübscher et al., 1997). The levee surface rises ~50 m above the thalweg of the meandering channel that is well imaged with multibeam bathymetry. Site U1454 is intended to provide a sequence through a channel-levee system that can be dated by ^{14}C and $\delta^{18}O$ and thereby be related to global climatic and sea-level cycles and other proxies for sediment flux and weathering. The general objective of the Pleistocene transect at 8°N is to document depocenter migration and overall accumulation rates since the Pliocene, and Site U1454 completes this approach by focusing on the Late Pleistocene and Holocene fan deposition. Obtaining a high-resolution levee record that could extend into the Holocene will allow comparison of this middle fan deposition to an upper fan levee likely constructed across the same channel levee at 16°N since 18 ka (Hübscher et al., 1997; Weber et al., 1997). Obtaining information on how the fan system developed during the last glacial cycle will provide insight into the relation of fan growth, sea-level change, and erosion changes driven by well-constrained climate evolution. The levee at 16°N records changing weathering and vegetation conditions since the Last Glacial Maximum (Galy et al., 2008; Lupker et al., 2013) that can be correlated to Site U1454.

Principal results

Site U1454 provides a key expanded section to the overall understanding of depositional processes in the Pleistocene Bengal Fan. This site was added during the expedition because of the inferred Holocene age of the channel with sediments suitable for dating with oxygen isotopes and radiocarbon or foraminiferal tests and on terrestrial organic material, in addition to high-resolution nannofossil biostratigraphic work. Accordingly, we will be able to determine the time spans over which the levee units have formed. Also, the surficial calcareous clay unit will constrain the timing of turbidite input at this location. Furthermore, we expect a high-resolution record that will allow us to link channel activity with sea level and glacial–interglacial climatic cycles.

Beneath the levee unit, coring recovered a sand-rich section comparable to Site U1452 that likely represents the progradational facies of early channel formation and erosion. Several other smaller channel systems in the vicinity contributed to sediment accumulation at Site U1454, and it will be interesting to investigate their temporal relationships with the active channel. Mud turbidites, silt, and sand beds are intercalated between hemipelagic units, indicating episodic channel activity.

An organic-rich turbidite was recovered at ~34 m core depth below seafloor (CSF-A) in the sand-rich section. It comprises an 18 cm thick layer of organic debris deposited at the base of a sand layer. The base of the organic layer contains a centimeter-sized wood branch. Unlike the Miocene and Pliocene, organic debris is not frequently found in Pleistocene turbidites, and this one represents an unusual transport from the delta to the fan. Identification of wood species may constrain the source of this deposit and the vegetation zone from which is derived.

[1] France-Lanord, C., Spiess, V., Klaus, A., Adhikari, R.R., Adhikari, S.K., Bahk, J.-J., Baxter, A.T., Cruz, J.W., Das, S.K., Dekens, P., Duleba, W., Fox, L.R., Galy, A., Galy, V., Ge, J., Gleason, J.D., Gyawali, B.R., Huyghe, P., Jia, G., Lantzsch, H., Manoj, M.C., Martos Martin, Y., Meynadier, L., Najman, Y.M.R., Nakajima, A., Ponton, C., Reilly, B.T., Rogers, K.G., Savian, J.F., Schwenk, T., Selkin, P.A., Weber, M.E., Williams, T., and Yoshida, K., 2016. Site U1454. *In* France-Lanord, C., Spiess, V., Klaus, A., Schwenk, T., and the Expedition 354 Scientists, *Bengal Fan*. Proceedings of the International Ocean Discovery Program, 354: College Station, TX (International Ocean Discovery Program). http://dx.doi.org/10.14379/iodp.proc.354.108.2016
[2] **Expedition 354 Scientists' addresses.**
MS 354-108: Published 7 September 2016

Site U1454 also completes the recovery of the Middle Pleistocene hemipelagic interval to the westernmost position and allows detailed study of the transition to intensified fan activity over a lateral distance of 300 km. This will shed light on the distances over which the active channel can deliver fine particles and contribute to the dilution of pelagic accumulation.

Operations

Four holes were cored at Site U1454. Hole U1454A is a single mudline core to 7.5 m drilling depth below seafloor (DSF) for microbiology and geochemical studies. Hole U1454B was cored with the advanced piston corer (APC) and half-length APC (HLAPC) systems to 161.8 m DSF and recovered 129.51 m of sediment (88%). This hole also included three 4.8 m advances without coring. The four upper cores utilized the APC system with an orientation tool and nonmagnetic hardware. Holes U1454C and U1454D were shallow penetrations (37.2 and 37.1 m DSF, respectively) and recovered 30.16 and 24.46 m of sediment (81% and 66%, respectively). The latter were cored to fully record the uppermost levee, provide sufficient samples for high-resolution studies, and avoid gaps. Cores from Holes U1454C and U1454D were not split during the expedition; they will be split following the expedition at the International Ocean Discovery Program (IODP) core repository.

Lithostratigraphy

Coring at Site U1454 recovered a full levee sequence most probably associated with the modern active channel of the Bengal Fan. The sequence is well represented by the 25 m sequence of mud turbidites in Unit II. Intervals of calcareous clay occur in the top 20 cm of Hole U1454B and are rare to about 110 m CSF-A. Deeper calcareous and clastic units alternate to 139.14 m CSF-A, where an 18 m thick interval of mottled calcareous clay with occasional color banding appears. Plant fragments occur in several silt intervals, including large (~2 cm) wood fragments. In the lower hemipelagic interval, one 8 cm thick volcanic ash layer is present at 145.5 m CSF-A. It is much thinner than the shallowest ash layers recovered at other Expedition 354 sites (~20 cm) and is likely related to the Toba eruption before the Brunhes/Matuyama boundary (790 ka).

Overall, siliciclastic units (silt, clay, and sand) at Site U1454 are compositionally classified as mica rich (muscovite and biotite) and quartz rich. Sand occurs mostly in fine to medium grain size ranges, with rare occurrences of coarse-grained particles. Feldspars and heavy minerals (e.g., amphibole, garnet, clinozoisite, zoisite, tourmaline, zircon, rutile, epidote, sillimanite, chloritoid, pyroxene, staurolite, and opaque minerals) are common in silt- and sand-rich layers and occasionally contain euhedral carbonate minerals and carbonate aggregate grains. Lithic fragments (e.g., biotite-gneiss, amphibole-mica schist, sillimanite-biotite-gneiss, and phyllite fragments) appear in sand. These minerals are consistent with a general provenance from Himalayan river sands (e.g., Garzanti et al., 2004).

Biostratigraphy

The levee system targeted for drilling at Site U1454 was expected to be of Pleistocene age. Biostratigraphic age control within the Pleistocene is limited to three nannofossil zones and two foraminiferal biomarkers (at 0.61 and 1.88 Ma). Calcareous nannofossil assemblages were observed in 44 samples from Site U1454, and the sediments contain a recent to early Pleistocene sequence. Foraminiferal assemblages were observed in 19 samples, and 19 samples were barren of foraminifers because of the recovery of turbidite sands in core catcher samples. Postexpedition work on nannofossils may further constrain sediment ages, as there are additional biostratigraphic markers that could potentially be used to refine the Pleistocene age model.

Paleomagnetism

We identified the Brunhes/Matuyama boundary and the Jaramillo and Cobb Mountain Subchrons in hemipelagic calcareous clay at 145–151 m CSF-A at Site U1454; they can be correlated with similar intervals in other holes within the Expedition 354 transect based on both magnetostratigraphy and seismic stratigraphy. The Brunhes/Matuyama boundary occurs at 145.83 m CSF-A, roughly similar to the depth of the same transition at Site U1453; as at Site U1453, the transition is associated with an ash layer. The upper boundary of the Jaramillo Subchron is likely in an interval that was not recovered between Cores 354-U1454B-29F and 30F. Core 30F contains the lower boundary of the Jaramillo Subchron (148.63 m CSF-A) and both boundaries of the Cobb Mountain Subchron (149.86–150.20 m CSF-A).

Physical properties

Physical property data were acquired on all Hole U1453A cores, including density, magnetic susceptibility, *P*-wave velocity, natural gamma radiation (NGR), and thermal conductivity. Physical property data from Site U1453 are mostly of good quality and reflect lithologic variations. Average physical properties were determined for five principal lithologies based on visual core description: the most common principal lithology is sand (~73 m), followed by clay (~45 m), calcareous clay (~23 m), and silt (~11 m), with volcanic ash occurring in traces. Wet bulk densities are rather uniform for terrigenous sediment (sand, silt, and clay), ranging from 1.89 to 1.96 g/cm^3. Calcareous clay has the lowest density (1.62 g/cm^3), followed by volcanic ash (1.68 g/cm^3). *P*-wave velocities are highest in sand (average = 1666 m/s) and lowest in silt and clay (~1530 m/s). Magnetic susceptibilities are also highest in sand (109×10^{-5} SI), followed by silt (90×10^{-5} SI) and clay (56×10^{-5} SI). The lowest values occur in calcareous clay (20×10^{-5} SI). NGR is high throughout the terrigenous components sand, silt, and clay (around 70 counts/s) and low in calcareous clay (43 counts/s). Thermal conductivity is highest in sand (1.82 W/[m·K]) and lowest in calcareous clay (1.17 W/[m·K]).

Geochemistry

At Site 1454, interstitial water measurements were conducted only on sediments from the top 7 m. As at other sites studied during this expedition, the hydrochemistry in this upper section is dominated by biogenic processes that release dissolved phosphate, ammonium, and CO_2 (leading to a rise in alkalinity) and consume sulfate.

Turbidites recovered at Site U1454 have $CaCO_3$ contents between 2 and 5 wt%, except for four samples from the upper 16 m of the levee that have $CaCO_3$ contents between 6 and 7.4 wt%. These four values are significantly higher than all carbonate content measured in turbidites from the seven Pleistocene sections cored during Expedition 354 (0.5–6 wt%). They are, however, identical to the carbonate content recorded in sediments deposited during the last deglaciation at the 17°N active channel-levee (Lupker et al., 2013). This could indicate a match between the 17°N and 8°N levee records; however, the pattern of K-depletion observed during the Holocene at 17°N was not observed at Site U1454.

Background and objectives

Site U1454 (see Figures **F3**, **F4**, and **F8** in the Expedition 354 summary chapter [France-Lanord et al., 2016d]) is the westernmost site of the transect of seven >200 m penetration holes drilled in the Middle Bengal Fan at 8°N during Expedition 354. This 300 km east–west transect is intended to provide an overview of Pleistocene fan architecture and evolution. This site was introduced during the expedition as an alternate site to better document recent and Late Pleistocene fan deposition. Expedition 354 sites in the eastern and central part of the transect revealed that fan deposition above and below the Toba ash layer (~70 ka) was remarkably low, marking the abandonment of fan between the Ninetyeast Ridge and 85°East Ridge for probably the last 300 ky.

Site U1454 is located ~50 km west of Site U1455 (DSDP Site 218) on the western levee of a channel-levee system believed to be the modern active channel of the fan (Hübscher et al., 1997). Site U1454 was intended to provide a sequence through a channel-levee system that could be dated by ^{14}C and $\delta^{18}O$ and which can thereby be related to global climatic and sea level cycles and other proxies for sediment flux and weathering. One primary objective was to determine when and how this channel migrated at this location and the sedimentary processes associated with the history of turbidity current activity in relation to recent climate changes.

The general objective of the Pleistocene transect at 8°N was to document depocenter migration and overall accumulation rates since the Pliocene, and Site U1454 addresses this objective by focusing on Late Pleistocene and Holocene fan deposition. Obtaining a high-resolution levee record that extends into the Holocene would allow comparison of this middle fan deposition to an upper fan levee likely constructed across the same channel levee at 16°30′N since 18 ka (Hübscher et al., 1997; Weber et al., 1997). The levee at 16°30′N shows consistently changing weathering and vegetation conditions since the Last Glacial Maximum (Galy et al., 2008; Lupker et al., 2012); these conditions can be further correlated at Site U1454.

Multibeam bathymetry shows the meandering, supposedly active channel north and east of Site U1454 at its outer levee (Figure **F1**). The levee surface rises ~50 m above the base of the channel. On the east side of the channel across from Site U1454, a point bar indicates recent westward channel migration. The meander loop must have shifted and evolved through time, and spillover deposition was likely quite variable at Site U1454.

Figure **F2** shows a portion of the transect seismic profile across Site U1454. The channel cross section reveals an asymmetric shape with a steep western flank (cut bar) and a westward migrating point bar at the eastern flank. The wedge-shaped geometry of the levee cored at Site U1454 is clearly visible with a maximum thickness of more than 30 m and a total width of ~15 km from the channel axis to each side. Below the levee are traceable marker horizons, which at other Expedition 354 sites typically represent longer periods of hemipelagic sedimentation that can be correlated through Site U1455 to the east.

Figure F1. Bathymetric and track chart, Site U1454. Projection is UTM Zone 45N. Multibeam bathymetry was acquired during R/V *Sonne* Cruises SO125 and SO188. Blue line = seismic Line SO125-GeoB97-027 with common depth point annotation. Contour interval is 20 m. A portion of the seismic profile is shown in Figure **F2** (red line, 22 km).

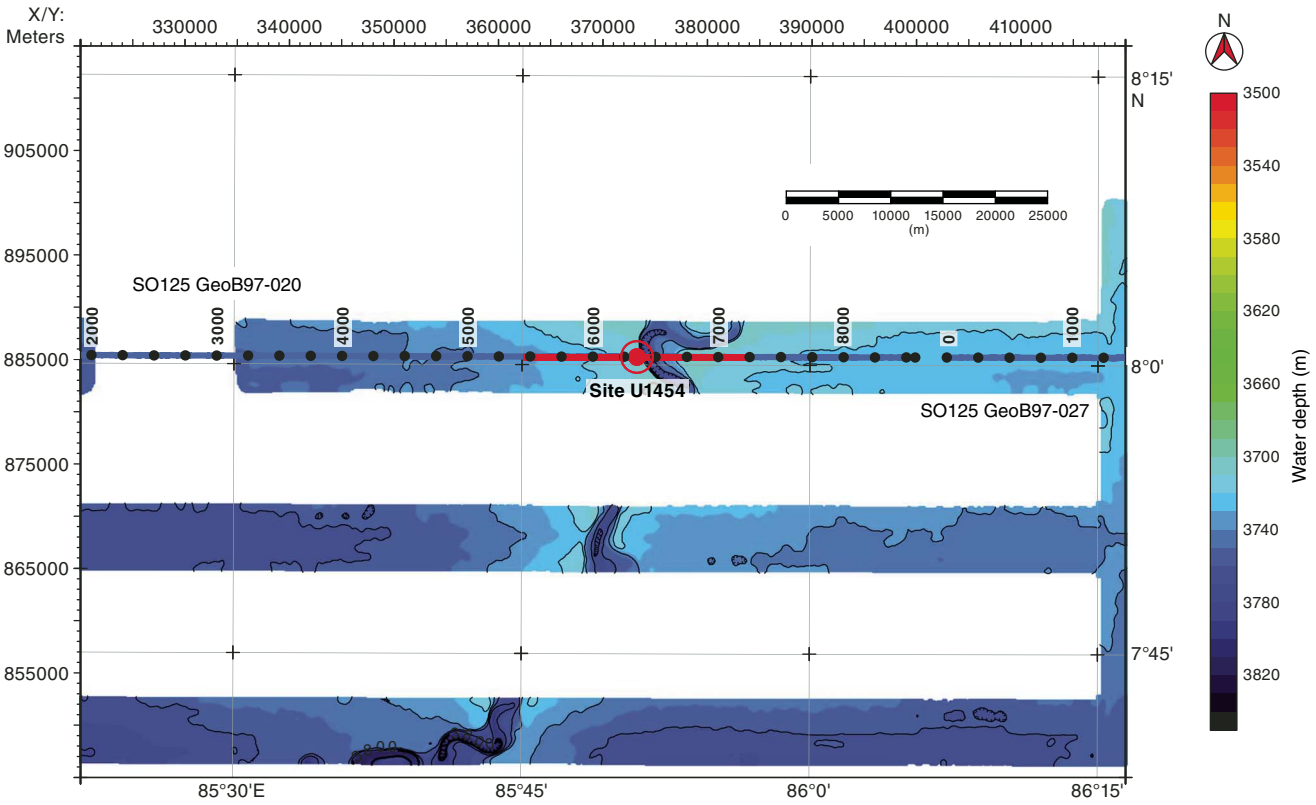

Figure F2. Seismic Line SO125-GeoB97-020, Site U1454. Total depth is 161.8 m DSF, assuming an average velocity of 1640 m/s.

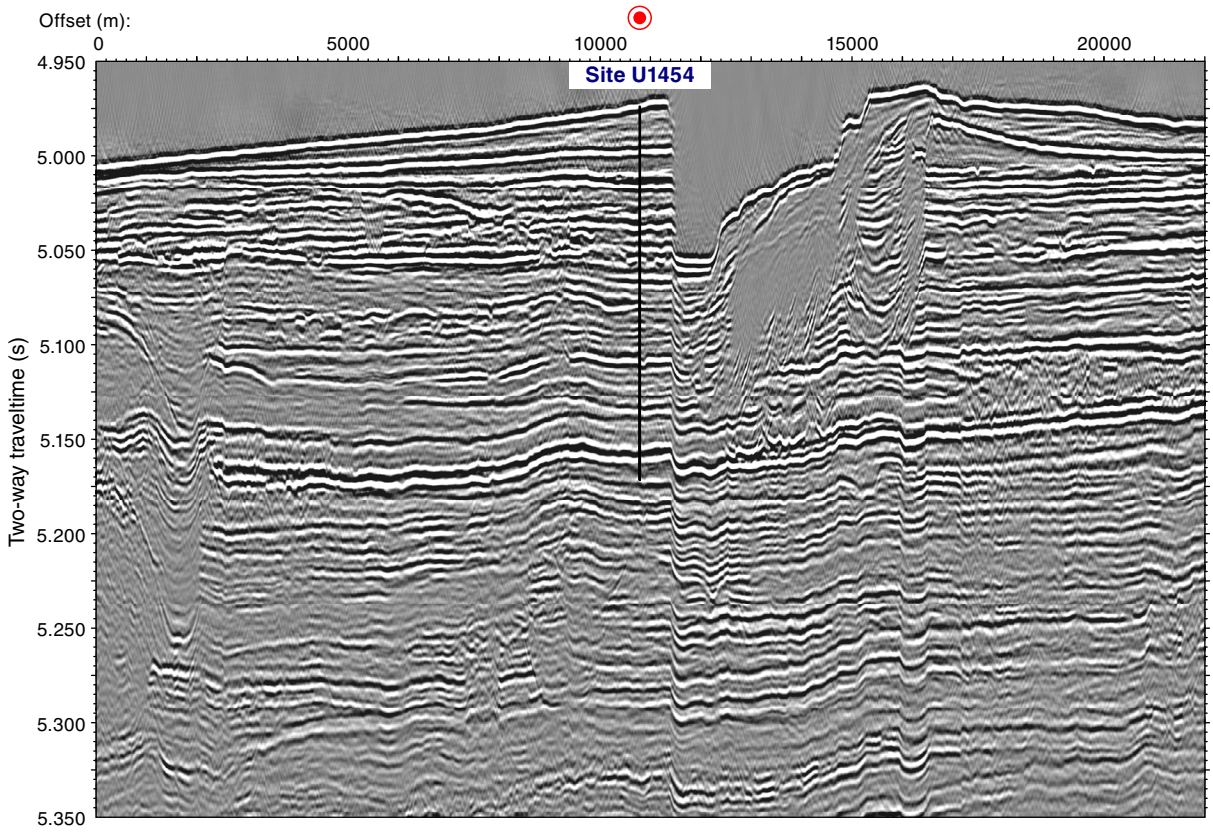

Operations

We cored four holes at Site U1454. Hole U1454A was a single mudline core to 7.5 m DSF for microbiology and geochemical studies. Hole U1454B was cored with the APC and HLAPC systems to 161.8 m DSF and recovered 129.51 m of sediment (88%). This hole also included three 4.8 m advances without coring. Holes U1454C and U1454D were shallow penetrations (37.2 and 37.1 m DSF, respectively) and recovered 30.16 m (81%) and 24.46 m (66%) of sediment, respectively. All cores, penetration depths, core recovery, and time recovered on deck are presented in Table **T1**. Core orientation was attempted for all APC cores, nonmagnetic hardware was used, and many of the cores were only partial strokes.

Hole U1454A

After a 56 nmi transit, we arrived at Site U1454 at 1706 h on 18 March 2015, assembled an APC/extended core barrel (XCB) bottom-hole assembly (BHA), and lowered it to the seafloor. At 0115 h on 19 March, we took a single mudline core in Hole U1454A (1H; 0–7.5 m DSF) for microbiologic and geochemical studies.

Hole U1454B

We offset the ship 20 m east and started coring in Hole U1454B at 0255 h on 19 March 2015. The APC penetrated from the seafloor to 32.1 m DSF (Cores 1H–4H; 30.28 m recovered; 94%). We switched to the HLAPC and cored from 32.1 to 161.8 m DSF. This 129.7 m interval included three 4.8 m advances without coring. Cores 5F–32F sampled 129.7 m of formation and recovered 99.23 m of sediment (86%). Coring was interrupted for 2 h (1400–1600 h on 19 March) when a broken strand on the coring line snagged in the top drive; ~1500 m of coring line had to be cut off. A single temperature measurement was obtained while recovering Core 30F.

Holes U1454C and U1454D

Having achieved our depth objectives, we decided to core two more holes to obtain a more complete section in the upper ~37 m. We pulled the bit out of Hole U1454B, offset the ship 20 m south, and started coring in Hole U1454C at 1650 h on 20 March 2015. Cores 1H–6F penetrated to 37.2 m DSF and recovered 30.16 m (81%). We pulled the bit out of Hole U1454C, offset the ship 20 m west, and started coring in Hole U1454D at 0020 h on 21 March. Cores 1H–5F penetrated to 37.1 m DSF and recovered 24.46 m (66%). We pulled the bit out of the seafloor (0630 h) and retrieved the drill string. Once the bit was back on the rig floor, we secured the rig floor, raised the thrusters, and departed for Site U1455 at 1336 h.

Table T1. Site U1454 core summary. * = APC cores with full-stroke; all others were partial strokes. DRF = drilling depth below rig floor, mbsl = meters below sea level, DSF = drilling depth below seafloor. H = advanced piston corer, F = half-length APC, X = extended core barrel. (Continued on next page.) **Download table in .csv format.**

Hole U1454A
Latitude: 8°0.4067′N
Longitude: 85°50.9882′E
Time on hole (days): 0.4 (9.00 h)
Seafloor (drill pipe measurement below rig floor, m DRF): 3721.0
Distance between rig floor and sea level (m): 11.1
Water depth (drill pipe measurement from sea level, mbsl): 3709.9
Total penetration (drilling depth below seafloor, m DSF): 7.5
Total depth (drill pipe measurement from rig floor, m DRF): 3728.5
Total length of cored section (m): 7.5
Total core recovered (m): 7.54
Core recovery (%): 101
Drilled interval (m): 0.0
Total number of cores: 1

Hole U1454B
Latitude: 8°0.4083′N
Longitude: 85°51.0025′E
Time on hole (days): 1.6 (37.5 h)
Seafloor (drill pipe measurement below rig floor, m DRF): 3721.4
Distance between rig floor and sea level (m): 11.1
Water depth (drill pipe measurement from sea level, mbsl): 3710.3
Total penetration (drilling depth below seafloor, m DSF): 161.8
Total depth (drill pipe measurement from rig floor, m DRF): 3883.2
Total length of cored section (m): 147.4
Total core recovered (m): 129.51
Core recovery (%): 88
Drilled interval (m): 14.4
Total number of cores: 29

Hole U1454C
Latitude: 8°0.3868′N
Longitude: 85°51.0033′E
Time on hole (days): 0.3 (8 h)
Seafloor (drill pipe measurement below rig floor, m DRF): 3721.4
Distance between rig floor and sea level (m): 11.1
Water depth (drill pipe measurement from sea level, mbsl): 3710.3
Total penetration (drilling depth below seafloor, m DSF): 37.2
Total depth (drill pipe measurement from rig floor, m DRF): 3758.6
Total length of cored section (m): 37.2
Total core recovered (m): 30.16
Core recovery (%): 81
Drilled interval (m): 0.0
Total number of cores: 6

Hole U1453D
Latitude: 8°0.3975′N
Longitude: 85°5.9927′E
Time on hole (days): 0.6 (14.00 h)
Seafloor (drill pipe measurement below rig floor, m DRF): 3721.8
Distance between rig floor and sea level (m): 11.1
Water depth (drill pipe measurement from sea level, mbsl): 3710.7
Total penetration (drilling depth below seafloor, m DSF): 37.1
Total depth (drill pipe measurement from rig floor, m DRF): 3758.9
Total length of cored section (m): 37.1
Total core recovered (m): 24.46
Core recovery (%): 66
Drilled interval (m): 0.0
Total number of cores: 5

Core	Top of cored interval DSF (m)	Bottom of cored interval DSF (m)	Interval cored (m)	Interval advanced without coring (m)	Core recovered length (m)	Curated length (m)	Recovery (%)	Date on deck (mm/dd/yy), time on deck UTC (h)	Date on deck (mm/dd/yy), time on deck UTC + 6 (h) (ship local time)
354-U1454A-									
1H*	0	7.5	7.5	—	7.54	7.54	101	03/18/15 2005	03/19/15 0205
		Totals:	7.5	—	7.54		101		
354-U1454B-									
1H*	0.0	7.1	7.1		7.10	7.10	100	03/18/15 2130	03/19/15 0330
2H*	7.1	16.6	9.5		8.93	8.93	94	03/18/15 2250	03/19/15 0450
3H*	16.6	26.1	9.5		8.85	8.85	93	03/18/15 2355	03/19/15 0555
4H	26.1	32.1	6.0		5.40	5.40	90	03/19/15 0100	03/19/15 0700
5F	32.1	34.6	2.5		2.44	2.44	98	03/19/15 0230	03/19/15 0830
6F	34.6	39.3	4.7		3.38	3.38	72	03/19/15 0330	03/19/15 0930
7F	39.3	44.0	4.7		4.13	4.13	88	03/19/15 0435	03/19/15 1035
8F	44.0	48.7	4.7		4.56	4.56	97	03/19/15 0540	03/19/15 1140
9F	48.7	53.4	4.7		4.48	4.48	95	03/19/15 0640	03/19/15 1240
10F	53.4	58.1	4.7		4.07	4.07	87	03/19/15 0740	03/19/15 1340
11F	58.1	62.8	4.7		4.75	4.75	101	03/19/15 1110	03/19/15 1710
12F	62.8	67.5	4.7		3.75	3.75	80	03/19/15 1215	03/19/15 1815
131	67.5	72.3		4.8	*****Drilled interval*****			03/19/15 1230	03/19/15 1830
14F	72.3	77.0	4.7		3.66	3.66	78	03/19/15 1315	03/19/15 1915
151	77.0	81.8		4.8	*****Drilled interval*****			03/19/15 1335	03/19/15 1935
16F	81.8	86.5	4.7		4.01	4.01	85	03/19/15 1435	03/19/15 2035
171	86.5	91.3		4.8	*****Drilled interval*****			03/19/15 1450	03/19/15 2050
18F	91.3	96.0	4.7		1.38	1.38	29	03/19/15 1540	03/19/15 2140
19F	96.0	100.7	4.7		2.06	2.06	44	03/19/15 1700	03/19/15 2300
20F	100.7	105.4	4.7		4.32	4.32	92	03/19/15 1815	03/20/150015
21F	105.4	110.1	4.7		3.51	3.51	75	03/19/15 1930	03/20/15 0130
22F	110.1	114.8	4.7		4.67	4.67	99	03/19/15 2040	03/20/15 0240
23F*	114.8	119.5	4.7		4.92	4.92	105	03/19/15 2150	03/20/15 0350
24F*	119.5	124.2	4.7		4.56	4.56	97	03/19/15 2300	03/20/15 0500
25F	124.2	128.9	4.7		2.52	2.52	54	03/20/15 0010	03/20/15 0610
26F	128.9	133.6	4.7		4.10	4.10	87	03/20/15 0115	03/20/15 0715
27F	133.6	138.3	4.7		4.56	4.56	97	03/20/15 0220	03/20/15 0820
28F*	138.3	143.0	4.7		4.73	4.73	101	03/20/15 0335	03/20/15 0935
29F*	143.0	147.7	4.7		4.85	4.85	103	03/20/15 0440	03/20/15 1040
30F*	147.7	152.4	4.7		5.16	5.16	110	03/20/15 0600	03/20/15 1200
31F*	152.4	157.1	4.7		4.93	4.93	105	03/20/15 0710	03/20/15 1310

Table T1 (continued).

Core	Top of cored interval DSF (m)	Bottom of cored interval DSF (m)	Interval cored (m)	Interval advanced without coring (m)	Core recovered length (m)	Curated length (m)	Recovery (%)	Date on deck (mm/dd/yy), time on deck UTC (h)	Date on deck (mm/dd/yy), time on deck UTC + 6 (h) (ship local time)
32F	157.1	161.8	4.7		3.73	3.73	79	03/20/15 0820	03/20/15 1420
		Totals:	147.4	14.4	129.51		88		
354-U1454C-									
1H*	0	4.1	4.1	—	4.07	4.07	99	03/20/15 1115	03/20/15 1715
2H*	4.1	13.6	9.5	—	9.41	9.41	99	03/20/15 1225	03/20/15 1825
3H*	13.6	23.1	9.5	—	9.16	9.16	96	03/20/15 1340	03/20/15 1940
4F*	23.1	27.8	4.7	—	3.53	3.53	75	03/20/15 1445	03/20/15 2045
5F	27.8	32.5	4.7	—	2.61	2.61	56	03/20/15 1555	03/20/15 2155
6F	32.5	37.2	4.7	—	1.38	1.38	29	03/20/15 1700	03/20/15 2300
		Totals:	37.2	—	30.16		81		
354-U1454D-									
1H*	0	8.7	8.7	—	8.68	8.68	100	03/20/15 1855	03/21/15 055
2H*	8.7	18.2	9.5	—	8.26	8.26	87	03/20/15 2015	03/21/15 215
3H*	18.2	27.7	9.5	—	0.00	0.00	0	03/20/15 2130	03/21/15 330
4F	27.7	32.4	4.7	—	3.87	3.87	82	03/20/15 2245	03/21/15 445
5F	32.4	37.1	4.7	—	3.65	3.65	78	03/20/15 2355	03/21/15 555
		Totals:	37.1	—	24.46		66		

Lithostratigraphy

Four holes were cored at Site U1454. Hole U1454A penetrated to 7.5 m DSF with 101% recovery. Hole U1454B penetrated to 161.8 m DSF (cored interval: 174.4 m with 88% recovery). Hole U1454C penetrated to 37.2 m DSF (cored interval: 37.2 m with 81% recovery). Hole U1454D penetrated to 37.1 m DSF (cored interval: 37.1 m with 66% recovery). Cores from Holes U1454C and U1454D were not split and are not described in this report. Hole U1454A overlaps with Hole U1454B to 7.49 m CSF-A. The overall dominant lithology for Site U1454 (Holes U1454A and U1454B only; 82% of total recovered material) is fine sand, silt, and clay, some with fining-upward sequences (i.e., turbidites). Calcareous clay comprises most of the remaining 18% of total recovered material; volcanic ash constitutes <1% and represents one thin (8 cm) glassy layer.

Hole U1454B cored through the western levee of what is thought to be the modern active channel system on the fan. Recovered sediments from Site U1454 are divided into seven lithostratigraphic units based on lithologic characteristics from macroscopic description, smear slide analyses, and physical property measurements (Figure **F3**; Table **T2**).

Unit summaries

Summaries of individual units are presented here, with more detailed descriptions in the following section.

Unit I is dominated by bioturbated clay intercalated with a few thin bioturbated silt layers. Nannofossil-rich calcareous clay covers the unit.

Unit II is composed of two subunits containing successions of mud turbidites separated by a ~1 m thick intercalating calcareous clay interval. The lower subunit is mainly clay turbidites with thin basal silt laminae; silt turbidites in the upper subunit frequently display laminations and cross bedding and occasionally contain woody plant fragments up to 2 cm in length. This unit most likely represents the levee of the modern active channel.

Unit III is dominated by mica-rich silty fine-grained sand occasionally punctuated by thin intervals of mud turbidites. There is a thin (~4 cm) layer of nannofossil-rich calcareous clay in the center of the unit.

Unit IV contains calcareous clay with a few interbedded bioturbated clays. Intervals of laminated silt and some "soupy" sand comprise minor lithologies.

Unit V contains silty fine sand alternating with normally graded clayey silt and silty clay.

Unit VI is dominantly mottled calcareous clay with occasional clay and quartz-rich and feldspar-rich silt interbeds. This unit also contains the only volcanic ash layer at Site U1454, observed at 145.47–145.54 m CSF-A.

Unit VII contains silty mica-rich fine sand and two thin beds of silty clay and clayey silt.

Lithostratigraphic summary

Similar to other Expedition 354 sites, lithologic differences between units (Table **T3**) and variations in grain size and bed thickness reflect cycles of proximal turbidity current channel activity and abandonment. Sand intervals may represent interlevee "sheet flows" (e.g., Curray et al., 2003), whereas finer grained fractions are more likely preserved in leveed sections. Calcareous units reflect cessation of proximal channel activity and increased entrainment of siliciclastic material, changes in water column productivity, or changes in the oxidation/reduction horizons of the pore waters.

Coring at Site U1454 recovered a full levee sequence that is thought to be associated with the modern active channel of the Bengal Fan and is well represented by a 25 m sequence of mud turbidites in Unit II. Unit II shows a gradual upward transition toward Unit I, from parallel-laminated silt and clay turbidites to nannofossil-rich bioturbated calcareous clay with rare silt interbeds. Together, these two units may represent a period of levee construction followed by a period of lower terrigenous input. Below the levee deposits, a sand unit is occasionally interbedded with sequences of thin (~10 cm) mud turbidites. Calcareous and clastic units alternate from 110 to 139.14 m CSF-A, where an 18 m thick interval of mottled calcareous clay with occasional color banding appears. Plant fragments occur in several silt intervals, including large (~2 cm) woody pieces (Figure **F4**). Unit VI contains the only volcanic ash layer recovered at Site U1454, which corresponds to a polarity reversal at 0.781 Ma (see **Paleomagnetism**).

Figure F3. Lithostratigraphic summary, Hole U1454B. For legend, see Figure **F5** in the Expedition 354 methods chapter (France-Lanord et al., 2016a).

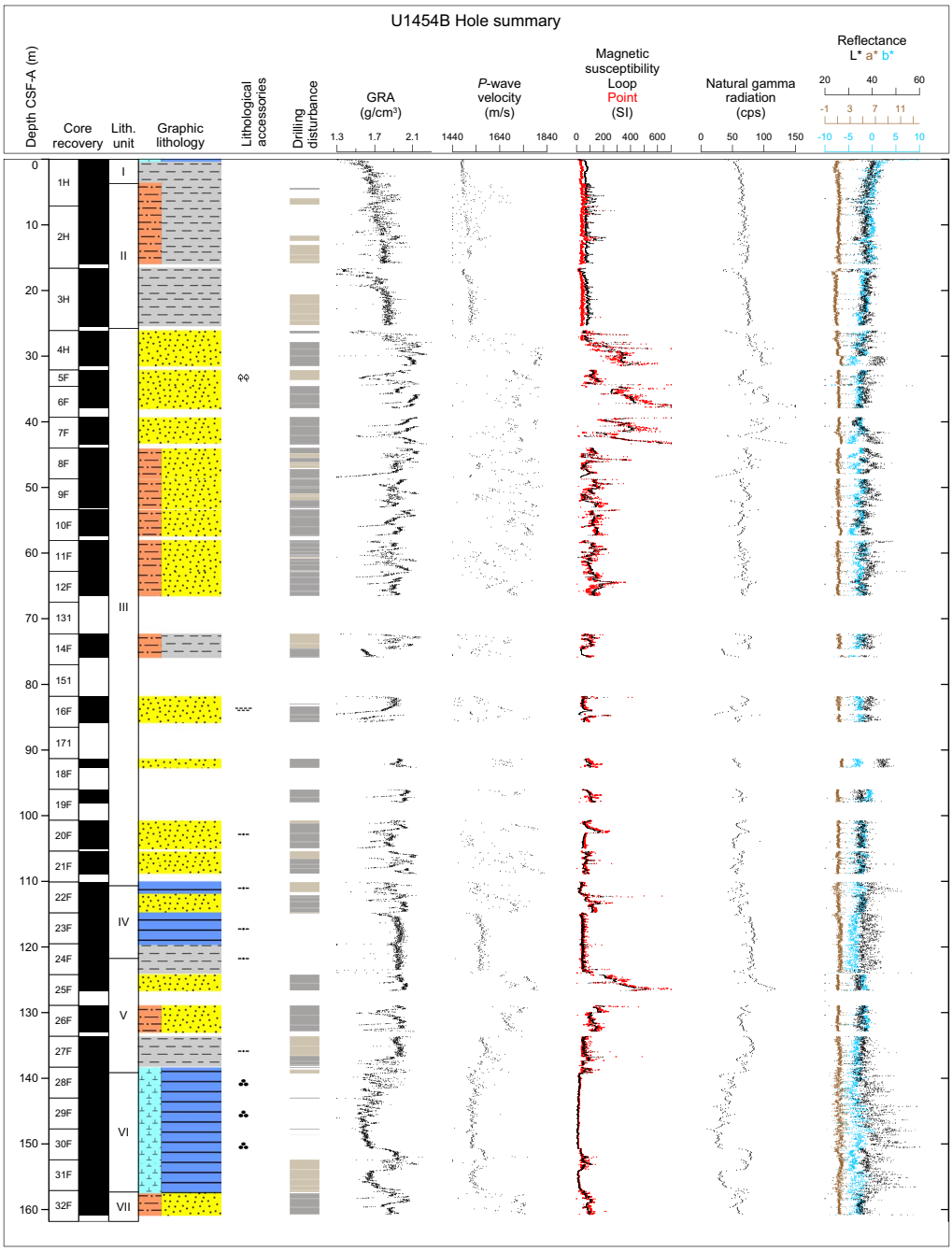

Table T2. Intervals, depths, major and minor lithologies, and ages of units, Site U1454. **Download table in .csv format.**

Unit	Interval	Top depth CSF-A (m)	Bottom depth CSF-A (m)	Major lithology	Minor lithology	Top age	Bottom age
	354-						
I	U1454A-1H-1, 0 cm, to 1H-3, 75 cm	0.00	3.75	Clay	Calcareous clay, silt	recent	Holocene(?)/mid-Late Pleistocene
	U1454B-1H-1, 0 cm, to 1H-3, 73 cm	0.00	3.73				
II	U1454A-1H-3, 75 cm, to 1H-CC, 10 cm	3.75	7.49	Silt, clay	Calcareous clay	Holocene(?)/mid-Late Pleistocene	mid-Late Pleistocene
	U1454B-1H-3, 73 cm, to 3H-CC, 15 cm	3.73	25.45				
III	U1454B-4H-1, 0 cm, to 22F-1, 57 cm	26.10	110.67	Sand	Silt, clay, calcareous clay	mid-Late Pleistocene	mid-Late Pleistocene
IV	U1454B-22F-1, 57 cm, to 24F-2, 75 cm	110.67	121.75	Calcareous clay	Sand, silt	mid-Late Pleistocene	mid-Late Pleistocene
V	U1454B-24F-3, 0 cm, to 28F-1, 84 cm	121.75	139.14	Sand	Silt, clay	mid-Late Pleistocene	mid-Late Pleistocene
VI	U1454B-28F-1, 84 cm, to 31F-CC, 23 cm	139.14	157.33	Calcareous clay	Sand, silt, clay, volcanic ash	mid-Late Pleistocene	early Pleistocene
VII	U1454B-32F-1, 0 cm, to 32F-CC, 5 cm	157.10	160.78	Sand	Silt, clay	early Pleistocene	early Pleistocene

Table T3. Core sections containing sand that were vertically settled on the core receiving platform, Site U1454. **Download table in .csv format.**

Core	Section	Top depth CSF-A (m)	Bottom depth CSF-A (m)
354-U1454B-			
6F	1	34.60	35.82
6F	2	35.82	37.22
6F	3	37.22	37.93
7F	1	39.30	40.69
7F	2	40.69	42.10
7F	3	42.10	43.38
8F	1	44.00	45.50
8F	2	45.50	47.00
8F	3	47.00	48.49
9F	1	48.70	49.84
9F	4	51.98	53.03
11F	1	58.10	59.18
11F	2	59.18	60.68
11F	3	60.68	61.80
11F	4	61.80	62.67
12F	1	62.80	63.71
12F	2	63.71	64.74
12F	3	64.74	65.83
12F	4	65.83	66.48
14F	3	74.62	75.85
16F	2	83.34	84.65
18F	1	91.30	92.65
19F	1	96.00	97.20
19F	2	97.20	97.95
21F	3	107.44	108.03
21F	4	108.03	108.87
25F	1	124.20	125.53
25F	2	125.53	126.67
32F	1	157.10	158.35
32F	2	158.35	159.66
32F	3	159.66	160.73
354-U1454C-			
5F	1	27.80	29.20
5F	2	29.20	30.26
6F	1	32.50	33.83
354-U1454D-			
5F	1	32.40	33.67
5F	2	33.67	34.95
5F	3	34.95	36.01

Figure F4. Black sand layer at the bottom of Section 354-U1454B-5F-2 containing large wood fragments. Sample was washed and air dried before imaging.

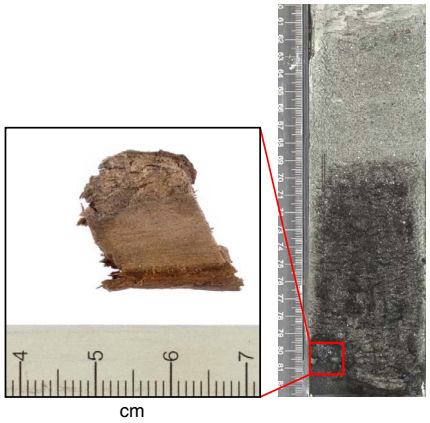

Overall, siliciclastic units (silt, clay, and sand) at Site U1454 are compositionally classified as mica rich (muscovite and biotite) and quartz rich. Sand occurs mostly in fine to medium grain size ranges, with rare occurrences of coarse-grained particles. Feldspar and heavy minerals (e.g., amphibole, garnet, clinozoisite, zoisite, tourmaline, zircon, rutile, epidote, sillimanite, chloritoid, pyroxene, staurolite, and opaque minerals) are common in silt- and sand-rich layers and occasionally contain euhedral carbonate minerals and carbonate aggregate grains. Lithic fragments (e.g., biotite-gneiss, amphibole-mica schist, sillimanite-biotite-gneiss, and phyllite fragments) appear in sand. From previous sites (see **Lithostratigraphy** in the Site U1451 chapter [France-Lanord et al., 2016b]), it is known that siliciclastic sediments in the fan contain between ~3% and 10% of detrital carbonate as well. Calcareous clays contain clay minerals, foraminifers, diatoms, and radiolarians.

The nomenclature for lithologic descriptions of fine sediments containing carbonate consists of a principal name and a modifier based on the composition estimated from visual description of the cores and from smear slide observations. The principal name of sediment that appears to contain >75% carbonate is calcareous ooze (see Figure **F4** in the Expedition 354 methods chapter [France-Lanord et al., 2016a]). The principal name of sediment that appears to contain <10% carbonate is clay. If sediment contains a mixture of clay-sized siliciclastic particles and calcareous components (i.e., carbonate contents between 10% and 75%), the principal name is calcareous clay. This nomenclature was adopted to describe the continuum of sediments recovered from almost pure clay to almost pure calcareous ooze. In most cases, lithologic names assigned using this protocol match well with measured carbonate content and accurately reflect the continuum of sediments recovered at this site. Examples can be seen in Figures **F6** in the Site U1451 chapter (France-Lanord et al., 2016b) and **F5** in the Site U1452 chapter (France-Lanord et al., 2016c).

Drilling disturbances at this site vary in intensity from slight to high and include flow-in, fractures, up-arching, soupy textures, and drilling biscuits. Flow-in is the most common drilling disturbance in fine-grained intervals, whereas sand may display a structureless (or soupy) texture. Core sections containing water-rich, loose, soupy sand were vertically settled on the catwalk and then normally curated, and as a result any grading or structures in these cores may be artificial and are not described here (Table **T3**). See Figure **F6** in the Expedition 354 methods chapter (France-Lanord et al., 2016a) for a more detailed description and graphic examples of drilling disturbance types.

Unit I

Intervals: 354-U1454A-1H-1, 0 cm, to 1H-3, 75 cm; 354-U1454B-1H-1, 0 cm, to 1H-3, 73 cm
Depths: Hole U1454A = 0–3.75 m CSF-A; Hole U1454B = 0–3.73 m CSF-A
Age: Holocene (?)/Middle–Late Pleistocene to recent
Lithology: clay (major); calcareous clay, silt (minor)

Description

This unit is dominated by light gray bioturbated clay intercalated with few very thin bioturbated silt layers and occasional mottled dark color bands. At the top of the unit, reddish to light brown nannofossil-rich calcareous clay occurs from the mudline to 0.22 m

Figure F5. Representative examples of major lithologies recovered in Hole U1454B. A. Light brown nannofossil-rich calcareous clay and greenish indurated layer (1H-1, 0–32 cm). B. Beds of dark gray silt fining upward into gray clay (mud turbidites; 1H-3, 31–113 cm). C. Greenish-gray bioturbated nannofossil-rich calcareous clay (3H-1, 58–90 cm). D. Dark gray soupy fine sand with mica (4H-3, 72–104 cm). E. Grayish white to light brown mottled calcareous clay (30F-1, 19–51 cm). F. Volcanic ash, 7 cm thick; color changes from black to light gray at the base to light brown upsection (29F-2, 85–117 cm).

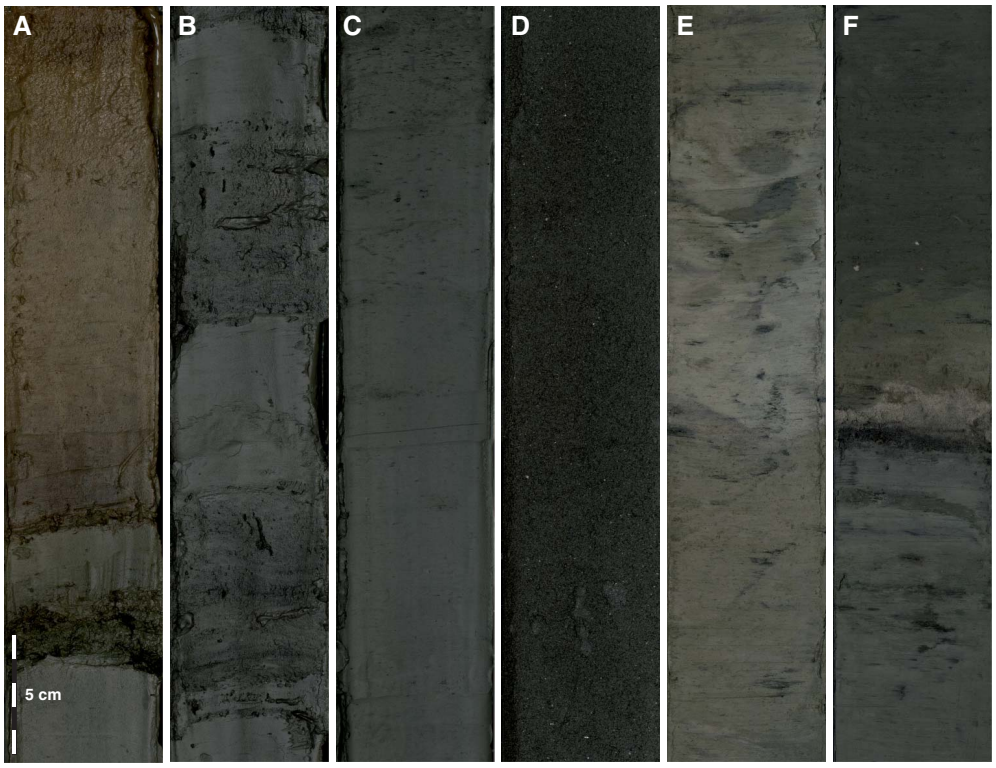

CSF-A, and a greenish indurated layer is found at 354-U1454B-1H-1, 25–27 cm (Figure F5A).

Composition from smear slides

See Figure F6 for representative smear slide images.

Nannofossil-rich calcareous clay

Nannofossils make up the major proportion (70%–90%) of this lithology, and aggregates of clay minerals, foraminifers, diatoms, and radiolarians comprise the minor proportion.

Clay

Clay mainly contains clay-sized detrital grains and clay minerals with small amounts of calcareous nannofossils. Occasionally, euhedral carbonate minerals are found. The smear slide of Sample 1H-1, 27 cm (0.27 m CSF-A) shows minor amounts of foraminifers (up to 10%) with clay minerals.

Unit II

Intervals: 354-U1454A-1H-3, 75 cm, to 1H-CC, 10 cm; 354-U1454B-1H-3, 73 cm, to 3H-CC, 15 cm
Depths: Hole U1454A = 3.75–7.49 m CSF-A; Hole U1454B = 3.73–25.45 m CSF-A
Age: Middle–Late Pleistocene to Holocene (?)
Lithology: clay, silt (major); calcareous clay (minor)

Description

This unit mostly consists of repeated fining-upward sequences from silt to clay (i.e., mud turbidites) (Figure F5B). The unit is divided into two subunits by an intercalated bioturbated nannofossil-rich calcareous clay bed from 354-U1454B-3H-1, 11 cm, to 3H-2, 98 cm (Figure F5C). The upper subunit is characterized by the frequent occurrence of medium- to thick-bedded silt-dominated turbidite beds, which show well-developed parallel and cross-lamination. The beds occasionally include plant fragments up to a few centimeters long and generally show two cycles of upward-thickening trends. The lower subunit is dominated by medium- to thick-bedded clay-dominated turbidite beds with basal very thin bedded silt layers or a solitary silt lamina. These beds often show black mottled bands near the top.

Figure F6. Representative examples of major lithologies in smear slides, Hole U1454B. A. Silty sand (9F-1, 11 cm; 48.8 m CSF-A). B. Sandy silt (9F-1, 20 cm; 48.9 m CSF-A). C. Clay (11F-2, 64 cm; 59.82 m CSF-A). D. Calcareous clay (29F-4, 58 cm; 147.43 m CSF-A; crossed nicols).

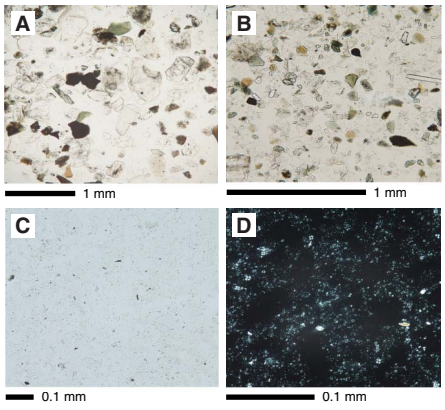

Composition from smear slides

See Figure F6 for representative smear slide images.

Calcareous clay

This lithology mainly contains clay-sized detrital grains, clay minerals, and calcareous nannofossils. Occasionally diatoms (3H-1, 30 cm; 16.90 m CSF-A) and foraminifers (3H-1, 17 cm; 16.77 m CSF-A) are recorded. Some intervals contain a high percentage of clay minerals, up to 80%.

Silty sand

Silty sand consists primarily of detrital grains, such as quartz, feldspar, lithic fragments, mica, and heavy minerals. Most grains are angular, except mica. The heavy mineral assemblage consists of amphibole, garnet, clinozoisite, zircon, epidote, zoisite, rutile, apatite, and opaque minerals. Occasionally, euhedral carbonate minerals and carbonate aggregate grains are found. The maximum grain size is 0.51 mm in diameter (1H-5, 51 cm; 6.51 m CSF-A).

Unit III

Interval: 354-U1454B-4H-1, 0 cm, to 22F-1, 57 cm
Depth: 26.10–110.67 m CSF-A
Age: Middle–Late Pleistocene
Lithology: silty fine sand (major); silty clay, clayey silt, calcareous clay (minor)

Description

Unit III consists mostly of dark gray soupy fine sands with mica (Figure **F5D**). Successions of dark gray silt fining upward into gray clay are occasionally found. Silt and clay beds are usually less than 10 cm thick. Sharp basal contacts of the silt beds, frequent parallel laminations of both clay and silt beds, and fining-upward textures (normal grading) characterize these intervals as successions of mud turbidites. Exceptionally large (>2 cm) and well-preserved wood fragments are found at the base of the sand layers toward the top 20 m of the unit (5F-2 and 5F-CC; Figure **F4**). Frequently occurring drilling disturbances are flow-in from the core bottom and up-arching. Section 9F-3 contains light brown nannofossil-rich calcareous clay with foraminifers.

Composition from smear slides

See Figure **F6** for representative smear slide images.

Calcareous clay

This lithology mainly contains clay-sized detrital grains, clay minerals, and nannofossils. Occasionally, radiolarians, diatoms, and foraminifers are recorded. Some intervals contain plant fragments (8F-1, 123 cm; 45.23 m CSF-A).

Silty sand

Silty sand consists primarily of detrital grains, such as quartz, feldspar, lithic fragments, mica, and heavy minerals. Most grains are angular except mica. The heavy mineral assemblage consists of amphibole, garnet, clinozoisite, zoisite, tourmaline, zircon, rutile, epidote, sillimanite, chloritoid, and opaque minerals. Occasionally, euhedral carbonate minerals and carbonate aggregate grains are found. Lithic fragments consist of biotite-gneiss, amphibole-mica schist, sillimanite-biotite-gneiss, and phyllite fragments. The maximum grain size is 0.69 mm in diameter (20F-2, 130 cm; 102.51 m CSF-A).

Clay

Clay minerals in this unit make up the significant proportion of total grains in this layer, with a minor amount of calcareous nannofossils and aggregates of carbonate grains.

Unit IV

Interval: 354-U1454B-22F-1, 57 cm, to 24F-2, 75 cm
Depth: 110.67–121.75 m CSF-A
Age: Middle–Late Pleistocene
Lithology: calcareous clay (major); fine sand, silt (minor)

Description

The major lithology, calcareous clay, is interbedded with thin and very thin beds of clay and is bioturbated (mottling and/or burrowed) throughout. In interval 23F-1, 0–50 cm, calcareous clay contains foraminifers. Silt has thin interbeds of clay, and in interval 22F-2, 38–150 cm, it exhibits parallel laminations. Fine sand is present in interval 22F-3, 38 cm, to 22F-4, 63 cm. Drilling disturbances at this site vary in intensity from slight to high and include up-arching and soupy textures. Fall-in is also present at the top of Core 23F.

Composition from smear slides

See Figure **F6** for representative smear slide images.

Silty sand

Silty sand consists primarily of quartz, feldspar, lithic fragments, mica, and heavy minerals. Most grains are angular except mica. The heavy mineral proportion contains amphibole, garnet, zoisite, tourmaline, epidote, clinozoisite, zircon, pyroxene, sillimanite, staurolite, rutile, sphene, and opaque minerals. The maximum grain size is 0.24 mm in diameter (22F-3, 90 cm; 114.00 m CSF).

Unit V

Interval: 354-U1454B-24F-3, 0 cm, to 28F-1, 84 cm
Depth: 121.75–139.14 m CSF-A
Age: Middle–Late Pleistocene
Lithology: silty fine sand (major); clay, silt (minor)

Description

Unit V is 17.39 m thick and comprises dark gray silty fine sand, gray silt, gray clay, dark gray silty clay, and dark gray clayey silt with mica. The thin clay beds are mottled and interbedded with silt laminae or thin beds. Some silt beds show a fining-upward texture (normally graded). Sands are homogeneous and soupy, which could indicate disturbance by drilling.

Composition from smear slides

See Figure **F6** for representative smear slide images.

Silty sand

Silty sand layers consist of quartz, feldspar, mica, and lithic fragments. Heavy minerals are mainly composed of amphibole, clinozoisite, zoisite, pyroxene, tourmaline, rutile, zircon, apatite, allanaite, sillimanite, and opaque minerals. Occasionally, euhedral carbonate minerals and nannofossils are found. The maximum grain size measurement is 0.42 mm in diameter (25F-2, 70 cm; 126.23 m CSF-A).

Unit VI

Interval: 354-U1454B-28F-1, 84 cm, to 31F-CC, 23 cm
Depth: 139.14–157.10 m CSF-A
Age: early to Middle–Late Pleistocene
Lithology: calcareous clay (major); volcanic ash, clay, silt, fine sand (minor)

Description

Unit VI mainly consists of grayish white to light brown mottled calcareous clay (Figure **F5E**). Light gray to black volcanic ash was observed at 29F-2, 97–104 cm (Figure **F5F**). The lower boundary of the ash layer is sharp, and the upper boundary is gradational and bioturbated. The interval from 30F-3, 0 cm, to 31F-1, 150 cm, is gray clay interbedded with light gray silt. The gray clays found in the upper meter of this interval contain calcareous nannofossils. The silt interbeds are well sorted and rich in quartz and feldspar. Coring disturbance is generally low in Unit VI and restricted to slight up-arching.

Composition from smear slides

See Figure **F6** for representative smear slide images.

Silty sand

Silty sand layers consist of quartz, feldspar, mica, and lithic fragments. Heavy minerals are mainly comprised of amphibole, garnet, zoisite, clinozoisite, pyroxene, sphene, rutile, zircon, apatite, chloritoid, sillimanite, staurolite, and opaque minerals. Occasionally, euhedral carbonate minerals are found. The maximum grain size measurement is 0.53 mm in diameter (30F-4, 36 cm; 152.06 m CSF-A).

Calcareous clay

This lithology mainly consists of calcareous nannofossils, ranging from 85% to 90% of total grains. Clay minerals, radiolarians, and foraminifers occur to a minor account. The top section of this unit additionally contains minor amounts of silt grains (28F-1, 87 cm; 139.17 m CSF-A). Lower amounts of radiolarians, foraminifers, and plant fragments are observed deeper in the interval (28F-2, 37 cm; 140.17). The deepest smear slide analyzed in this unit contains a higher proportion of clay minerals than calcareous nannofossils and rare foraminifers (31F-2, 75 cm; 154.65 m CSF-A).

Volcanic ash

The smear slide from the ash layer in this unit mainly consists of volcanic glass shards 0.02–0.50 mm in diameter. The typical range for the volcanic glass proportion is 90%–95% of the total grains, and phenocrysts mainly consist of quartz and minor amounts of biotite, feldspar, and hornblende. Volcanic glass appears in the form of clear plates, flakes, and strands with a relatively low refractive index (29F-2, 103 cm; 145.53 m CSF-A). Some slightly altered grains were also observed.

Unit VII

Interval: 354-U1454B-32F-1, 0 cm, to 32F-CC, 5 cm
Depth: 157.10–160.78 m CSF-A
Age: early Pleistocene
Lithology: silty sand (major); silty clay, clayey silt (minor)

Description

Unit VII is 3.68 m thick and comprises dark gray silty fine sand with mica. The upper portion of Section 32F-1 consists of two thin- to medium-bedded gray silty clay layers and a thin bed of dark gray clayey silt with mica. The sands are homogeneous and soupy, which could indicate disturbance by drilling.

Composition from smear slides

See Figure **F6** for representative smear slide images.

Sandy silt

Sandy silt consists primarily of quartz, feldspar, lithic fragments, mica, and heavy minerals. Heavy minerals consist predominantly of amphibole, garnet, zoisite, sphene, clinozoisite, epidote, zircon, rutile, sillimanite, chloritoid, and opaque minerals. The maximum grain size is 0.46 mm in diameter (32F-2, 45 cm; 158.8 m CSF-A).

Maximum grain size

Maximum grain size was determined at approximately 5 m intervals at Site U1454. In each case, the coarsest and/or thickest lithology in the individual core (generally from the base of the coarsest turbidite) was chosen for smear slide analysis, and the largest five equant detrital grains (quartz and feldspar) were measured. Results are shown in Figure **F7**. The maximum grain size ranges from 0.08 to 0.69 mm (very fine sand to coarse sand) and corresponds to the sand layer at the base of Unit III.

Figure F7. Maximum grain size, Hole U1454B.

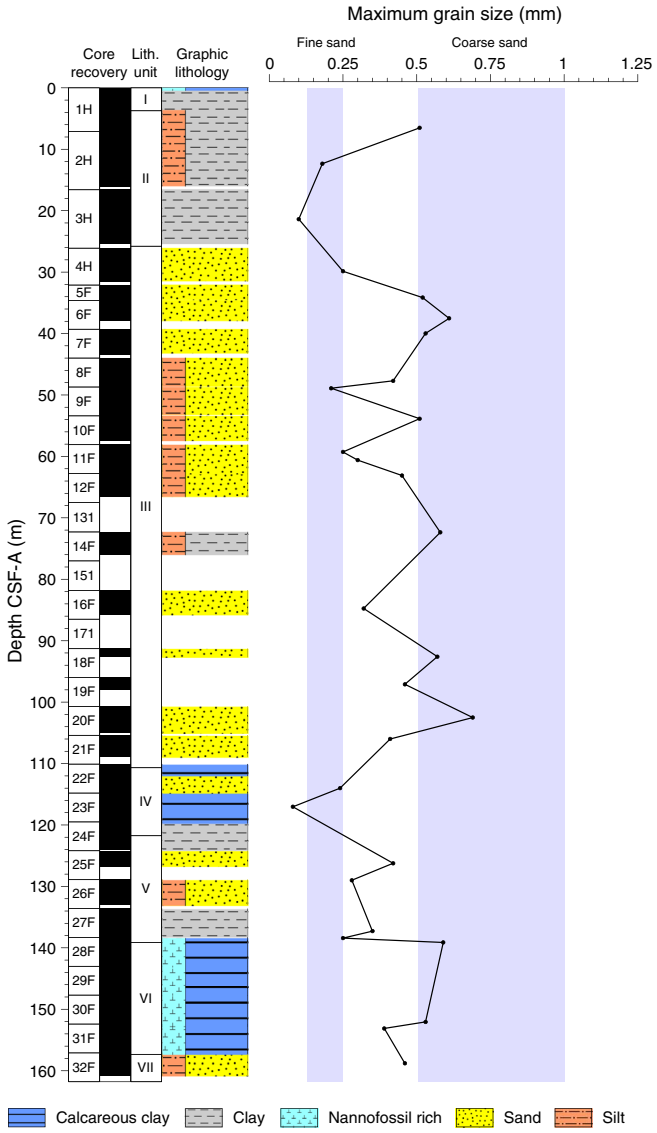

XRD data

Clay minerals were extracted from representative lithologies (sand, silt, clay, and calcareous clay).

The observed clay mineral assemblages from Holes U1454A and U1454B are mainly composed of illite, chlorite/vermiculite, smectite/mixed layers, and kaolinite. Illite and chlorite/vermiculite are the dominant clay minerals in all lithologies: calcareous clay (average = 60%–65%) and clay and sand samples (average = 20%). The clay assemblages observed at Site U1454 in the different lithologies do not show any evolution with depth (Figure **F8**), suggesting relatively stable sources and/or turbiditic transport processes. No change in clay mineralogy has been observed in the calcareous clay deposits. In conclusion, this assemblage appears similar to the illite-chlorite-rich clay assemblage documented in the distal fan (Leg 116) and modern rivers flowing from the Himalaya (Bouquillon et al., 1990).

Figure F8. Semiquantitative clay mineral proportions, Site U1454.

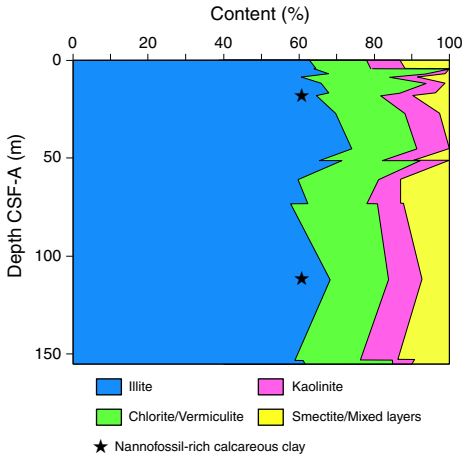

Biostratigraphy

Calcareous nannofossils and planktonic foraminifers provide biostratigraphic constraints at Site U1454 (Tables **T4**, **T5**, **T6**). Four biomarkers were identified at this site; they are listed in Table **T6** and integrated into Figure **F23**.

Calcareous nannofossils

Calcareous nannofossil assemblages were observed in 44 samples from Site U1454 (Table **T4**). Preservation is moderate to good, and group abundance ranges from very few to very abundant, with one barren sample.

Site U1454 sediments contain a recent to early Pleistocene sequence. The presence of *Emiliania huxleyi* in all samples from Holes U1454A, U1454C, and U1454D assigns them to calcareous nannofossil Zone NN21. Hole U1454B is differentiated into three nannofossil zones. Zone NN21 is based on the first occurrence (FO) of *E. huxleyi* in Sample 24F-CC. Zone NN20 is a gap zone between the FO of *E. huxleyi* and the last occurrence (LO) of *Pseudoemiliania lacunosa*. *P. lacunosa* was observed in Sample 27F-CC (138.11 m CSF-A), marking the top of Zone NN19.

Pleistocene nannofossil assemblages at this site are dominated by *Gephyrocapsa* spp., *Calcidiscus leptoporus*, and *Reticulofenestra* spp., with very few to few occurrences of *E. huxleyi*, *Helicosphaera* spp., *Ceratolithus* spp., and *Umbilicosphaera sibogae*.

Planktonic foraminifers

Site U1454 planktonic foraminiferal assemblages are characteristic of tropical–subtropical environments. Preservation is generally good to moderate, and fragmentation of planktonic foraminifers ranges from light to severe. The group and species abundances of planktonic foraminifers are recorded in Table **T5**. A planktonic foraminifer biostratigraphy was generated at Site U1454 from Hole U1454B using core catchers. Additionally, six samples from Hole U1454C and four samples from Hole U1454D were examined.

The sedimentary succession at this site ranges from Subzone PT1b (Middle–Late Pleistocene) to Zone PT1a (early Pleistocene) and agrees with the nannofossil biostratigraphy. A barren interval was identified in Hole U1452B between Samples 4H-CC (31.46 m CSF-A) and 12F-CC (66.48 m CSF-A), most likely due to recovery of turbidite sands in these core catchers.

Assemblages exhibited low diversity and were dominated by abundant *Neogloboquadrina dutertrei*, *Globigerinoides ruber*, and *Pulleniatina obliquiloculata*, with rare *Globigerina bulloides* and *Orbulina universa*. No major faunal turnovers occurred during this narrow time interval, and benthic foraminifers remain rare throughout (Table **T5**). The division between Subzones PT1b and PT1a is indicated by the top of *Globorotalia tosaensis* between Samples 27F-CC (138.11 m CSF-A) and 28F-CC (143.03 m CSF-A). The LO of *Globigerinoides obliquus* is between Samples 29F-CC (147.80 m CSF-A) and 30F-CC (152.68 m CSF-A). The top of this species has been calibrated by Chaisson and Pearson (1997) to 1.30 Ma.

Table T4. Calcareous nannofossils, Site U1454. **Download table in .csv format.**

Table T5. Planktonic foraminifer group and species abundance, Site U1454. **Download table in .csv format.**

Table T6. Biostratigraphic age datums and midpoint calculations, Site U1454. FO = first occurrence, LO = last occurrence. **Download table in .csv format.**

Top core, section	Bottom core, section	Zone	Marker event	GTS2012 age (Ma)	Top depth CSF-A (m)	Bottom depth CSF-A (m)	Midpoint depth CSF-A (m)	Depth CSF-A (m) ±
Planktonic foraminifer datums (Wade et al., 2011):								
354-U1454B-	354-U1454B-							
27F-CC	28F-CC	PT1a	LO *Globorotalia tosaensis*	0.61	138.11	143.03	140.57	2.46
Calcareous nannofossil datums (Gradstein et al., 2012):								
354-U1454B-	354-U1454B-							
24F-CC	25F-CC	NN21	FO *Emiliania huxleyi*	0.29	124.03	126.67	125.35	1.32
		NN20	Gap zone					
28F-CC	29F-CC	NN19	LO *Pseudoemiliania lacunosa*	0.44	132.95	138.11	135.53	2.58

Paleomagnetism

Paleomagnetic analyses at Site U1454 focused mainly on identifying magnetic polarity reversals and linking them to the geomagnetic polarity timescale (Gradstein et al., 2102) and on identifying intervals suitable for shore-based paleomagnetic work. All cores were collected with nonmagnetic APC or HLAPC barrels. Cores 354-U1454B-1H through 4H, 354-U1454C-1H through 3H, and 354-U1454D-1H through 2H were oriented using the Icefield MI-5 tool.

Archive section halves from 19 Hole U1454B cores were measured using the shipboard superconducting rock magnetometer (SRM). We took a conservative demagnetization approach and only measured the NRM without alternating field (AF) demagnetization for Brunhes Chron cores, preserving the remanent magnetization for shore-based research. In cores likely to be of magnetostratigraphic importance, section-half remanent magnetization was measured after 0, 10, 15, and 20 mT AF demagnetization at 2.5 cm intervals. Sections where the sediment was sandy, watery, or heavily disturbed by the coring process were not measured. We did not measure cores from any other hole because Core 354-U1454A-IH was heavily sampled for geochemistry and microbiology and cores from Holes U1454C and U1454D were not split on ship. Magnetic polarity interpretation below is based on remanence vectors measured after 20 mT AF treatment; sandy, soupy, and deformed intervals; section edges; and core tops are not interpreted (see **Paleomagnetism** in the Expedition 354 methods chapter [France-Lanord et al., 2016a]).

Ten discrete samples were collected to supplement the data from the archive section halves. Most of these samples were taken from core catchers in Brunhes Chron cores to assess the stability of remanence, magnetic mineralogy, and potential for shore-based study of relative paleointensity. The samples were measured on the JR-6A spinner magnetometer after 0, 10, 15, 20, 25, 30, 35, 40, 50, 60, and 80 mT AF treatments.

Results

Paleomagnetic results from both section-half and discrete measurements are presented in Figures **F9** and **F10** and Tables **T7** and **T8**. As at Sites U1449–U1453, both positive and negative inclinations are present in Hole U1454A. A vertical overprint, likely imparted by the drilling process, is in most cases demagnetized by AF demagnetization in peak fields of 10 mT. For the section halves subjected to 20 mT AF demagnetization, the median inclination is on average close to that expected from a geocentric axial dipole (GAD; median observed: 19.5°, expected: 15.7°) given the site's present-day location.

Stepwise AF demagnetization of discrete samples (Figure **F9**) and of a limited number of section halves indicates that Site U1454 sediments have a coercivity spectrum broadly similar to similar lithologies recovered at other Expedition 354 sites. Several discrete samples acquired a very large remanence in peak AF treatments above 40 mT. This is likely either gyroremanent magnetization (GRM) or anhysteretic remanent magnetization (ARM). The amount of remanence acquired during AF demagnetization appears to have little relationship with lithology; both silt and clay acquire a substantial remanence during AF treatment. Lighter colored sediments nearer the top of the hole acquire smaller GRM or ARM than darker colored sediments. Based on AF demagnetization of discrete samples, coercivities are consistent with magnetite and/or titanomagnetite as the principal NRM carrier. The specific magnetic mineralogy will be assessed further during postexpedition work.

Figure F9. NRM decay (left) and AF demagnetization vector (right) diagrams of discrete samples, Site U1454. Points on demagnetization vector diagrams = projected endpoints of the remanent magnetization vector measured for each sample in core coordinates (azimuth not oriented). A. Sample with ChRM vector with positive component inclination. Demagnetization behavior is consistent with magnetite or titanomagnetite as the principal NRM carrier. B. Deviation of remanence vector toward *Y*-direction indicates acquisition of remanence (likely GRM) during AF treatment.

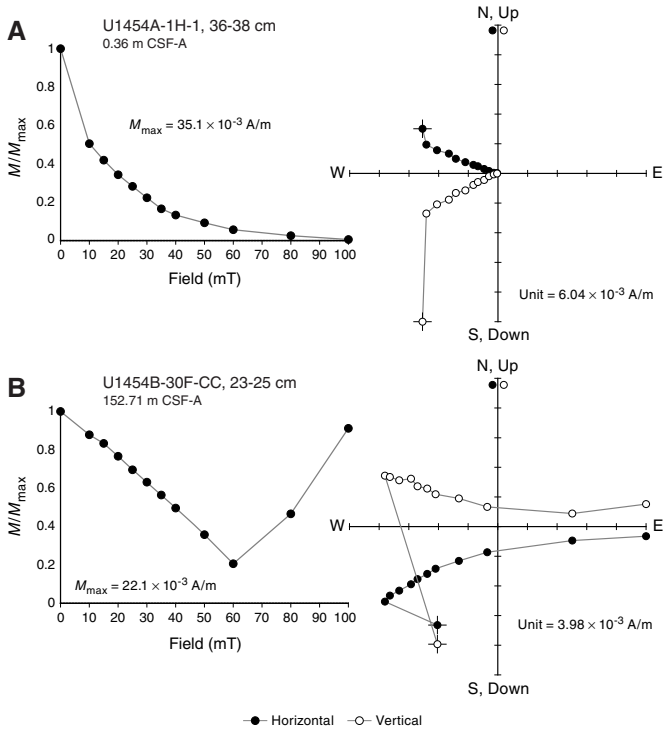

Magnetostratigraphy

Sediments from oriented Cores 354-U1454B-1H through 4H all have stable declinations that are indicative of normal polarity and appear to be suitable for more detailed shore-based analysis to investigate paleosecular variation and relative paleointensity (Table **T9**).

Core 354-U1454B-30F contains mixed polarity and can be correlated with the calcareous clay interval observed at roughly the same depth in Cores 354-U1450A-36F, 354-U1452B-37F, and 354-U1453A-31F and at somewhat shallower depths in Cores 354-U1449A-18F and 354-U1451A-13F. Three polarity reversals can be identified in Core 354-U1454B-30F on the basis of changes in declination (Figure **F11**; Table **T8**). We identify the bottom two as the upper and lower boundaries of the Cobb Mountain Subchron (C1r.2n; 1.173–1.185 Ma; Gradstein et al., 2012). A reversed to normal transition is identified using the Cobb Mountain Subchron as a reference for normal polarity. We identify this as the lower boundary of the Jaramillo Subchron (C1r.1n; 1.072 Ma). The upper Jaramillo is not observed in Hole U1454B and is likely located between the base of Core 29F and the top of Core 30F despite the fact that recovery was more than complete in these two cores.

As observed at Sites U1449 and U1451–U1453, a polarity change associated with an ash layer occurs in Section 354-U1454B-29F-2 (145.47–145.54 m CSF-A). We interpret this ash as Ash D of Dehn et al. (1991) and the polarity reversal as the Brunhes/Matuyama boundary (C1n-C1r; 0.781 Ma).

Figure F10. NRM of archive section halves and discrete samples before and after 20 mT AF demagnetization, Hole U1454B. Light gray dots = before demagnetization. Note that most section halves were not demagnetized. Dark gray circles = intervals that do not meet quality criteria (see **Paleomagnetism** in the Expedition 354 methods chapter [France-Lanord et al., 2016a]). Blue dots = calcareous clay, red dots = volcanic ash, black dots = other lithology. Inclination and declination: dark green dots = principal component directions from discrete samples. Inclination: gray lines either side of 0° = expected inclinations from GAD. Declination: yellow = oriented cores. Declinations are in a geographic reference frame only where orientation data are available. Intensity: intensity of magnetization before and after demagnetization. Large light green dots = before demagnetization, dark green dots = after demagnetization. Magnetic susceptibility (MS) = point measurements on archive section halves.

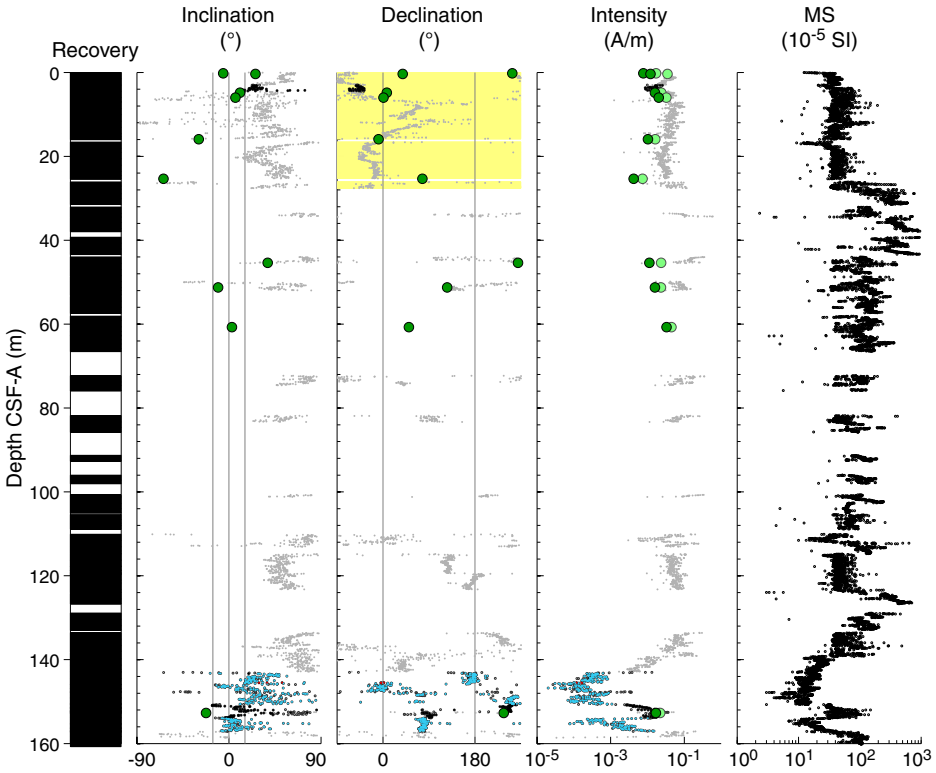

Table T7. ChRM of discrete samples, Site U1454. **Download table in .csv format.**

Table T8. Magnetostratigraphy, Hole U1454B. NR = not recovered. **Download table in .csv format.**

Polarity interval top depth CSF-A (m)	Top chron/ subchron age (Ma)	Chron/subchron	Comments
0.00	0.000	Bruhnes (C1n)	
145.83	0.781	Matuyama (C1r.1r)	Core 29F
NR	0.988	Jaramillo (C1r.1n)	Between bases of Cores 29F and 30F
148.63	1.072	Matuyama (C1r.2r)	Core30F
149.86	1.173	Cobb Mountain (C1r.2n)	Core 30F
150.20	1.185	Matuyama (C1r.3r)	Core 30F

Table T9. Orientation data, Site U1454. **Download table in .csv format.**

Hole	Core	Core type	Azimuthal orientation (°)	Fisher mean declination (°)	Mean oriented declination (°)	Comments
B	1	H	107.5	185.4	–67.1	Declination from 0 mT step
B	2	H	241.3	175.6	57.0	Declination from 0 mT step
B	3	H	310.9	23.8	–67.1	Declination from 0 mT step
B	4	H	297.1	31.2	–67.1	Declination from 0 mT step
C	1	H	122.9			Core not split during expedition
C	2	H	67.1			Core not split during expedition
C	3	H	324.1			Core not split during expedition
D	1	H	22.8			Core not split during expedition
D	2	H	3.6			Core not split during expedition

Figure F11. Polarity interpretation of Cores 354-U1454B-29F and 30F. Circles = measurements that do not pass quality control criteria (see **Paleomagnetism** in the Expedition 354 methods chapter [France-Lanord et al., 2016a]). Blue dots = calcareous clay, black dots = other lithology, green dots = measurements on discrete samples. Declination is rotated and illustrates magnetostratigraphic interpretation. A single vertical axis rotation was applied to the entire core so that points interpreted as normal polarity plot near the 0° line. Intensity = intensity of magnetization after 20 mT AF demagnetization. Magnetic susceptibility (MS) = point measurements on archive section halves. Polarity: black = normal, white = reversed, gray = uncertain. Geomagnetic polarity timescale (GPTS) of Gradstein et al. (2012).

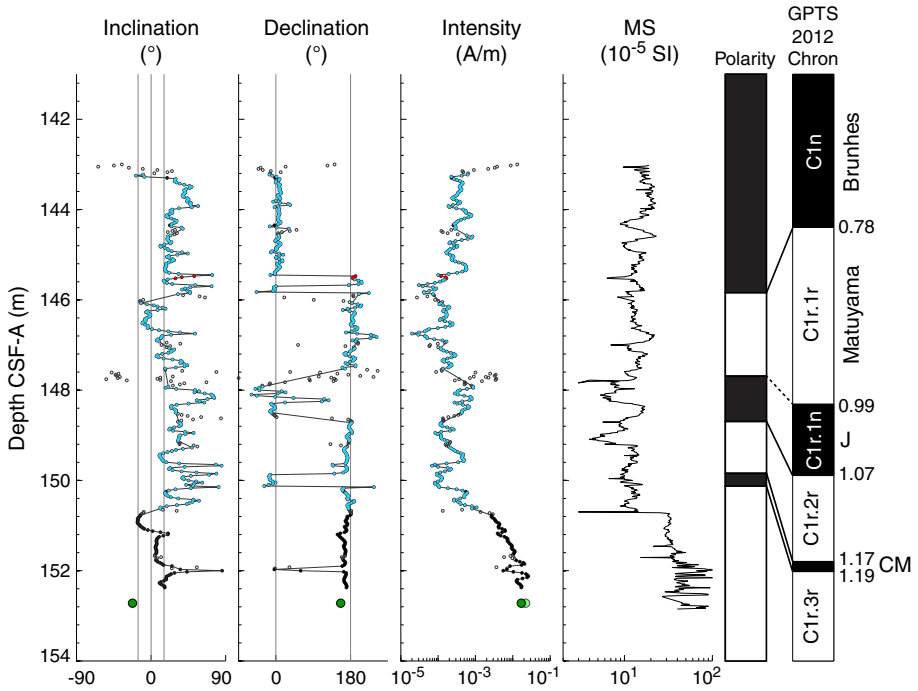

Geochemistry and microbiology

Hydrocarbon gas sampling and analysis

Headspace gas samples were taken at a frequency of one sample per core in Holes U1454A and U1454B as part of the routine safety monitoring program (Table **T10**). Low methane concentrations were observed at a single sampling point (4.5 m CSF-A) in Hole U1454A (7 ppmv) and from 0 to 101 m CSF-A in Hole U1454B (1 ppmv). In Hole U1454B, methane concentrations deeper than 101 m CSF-A increased and showed scatter (18–1816 ppmv) between 101 and 150 m CSF-A. At greater depths, methane concentrations dropped to 2 ppmv, measuring 9 ppmv at the bottom of the core.

Interstitial water sampling and chemistry

Twelve samples from Hole U1454A were analyzed for interstitial water chemistry (Table **T11**), focusing on microbiological processes happening in the uppermost 7 m of the sediment. As at other sites, the chemistry of the interstitial water in this upper portion of the sediment column is dominated by biogenic processes that release dissolved phosphate, ammonium, and CO_2 (leading to a rise in alkalinity) and consume sulfate. Near the water/sediment interface (0.1 m CSF-A), the sulfate content is indistinguishable from seawater composition, and its reduction happens at a constant rate and reaches 40% at 6.9 m CSF-A (Figure **F12**). Alkalinity increases (>400%) from the seafloor to 7 m CSF-A. In this interval, there is little change in calcium content, and magnesium content mimics that of calcium to 4 m CSF-A where the two cations diverge. This rise in magnesium content between 4 and 7 m CSF-A was not observed at any other sites and is difficult to explain. Salinity is within 0.5 of the values found in the near-surface sediments at Sites U1449–U1453 and barely changes in this interval. Phosphate and ammonium contents are not correlated at this site; phosphate peaks near the top, whereas ammonium only becomes noticeable when phosphate content is <9 µM.

Table T10. Methane concentrations, Holes U1454A and U1454B. **Download table in .csv format.**

Table T11. Interstitial water geochemical data, Site U1454. **Download table in .csv format.**

Bulk-sediment geochemistry

Inorganic carbon

Total inorganic carbon (TIC) concentrations were determined on 18 sediment samples from Holes U1454A and U1454B (Table **T12**; Figure **F13**). TIC values expressed as weight percent calcium carbonate ($CaCO_3$), assuming inorganic carbon is exclusively present as $CaCO_3$, range between 2.1 and 11.6 wt%. Turbiditic sediments are characterized by carbonate content varying between 2.1 and 11.4 wt% (i.e., covering the entire range of values measured at Site U1454). Within turbidites, no systematic covariation between grain size—as inferred from Al/Si ratios—and carbonate content was observed (at least in our small numbers of samples). In the uppermost 12 m CSF-A, five turbiditic sediments have carbonate content >6.0 wt%. This is very unusual in the context of the seven Pleistocene sections drilled along the transect at 8°N. Such elevated carbonate content in turbiditic sediment was only observed in one sample from the uppermost 200 m of Sites U1449–U1453 and DSDP Site 218 (von der Borch, Sclater, et al., 1974; Figure **F14**). However, turbiditic sediments with carbonate content above 6.0

Figure F12. Variations of salinity, bromide, sulfate, phosphate, ammonium, alkalinity, magnesium, calcium, sodium, potassium, and silicon concentrations in interstitial waters, Site U1454.

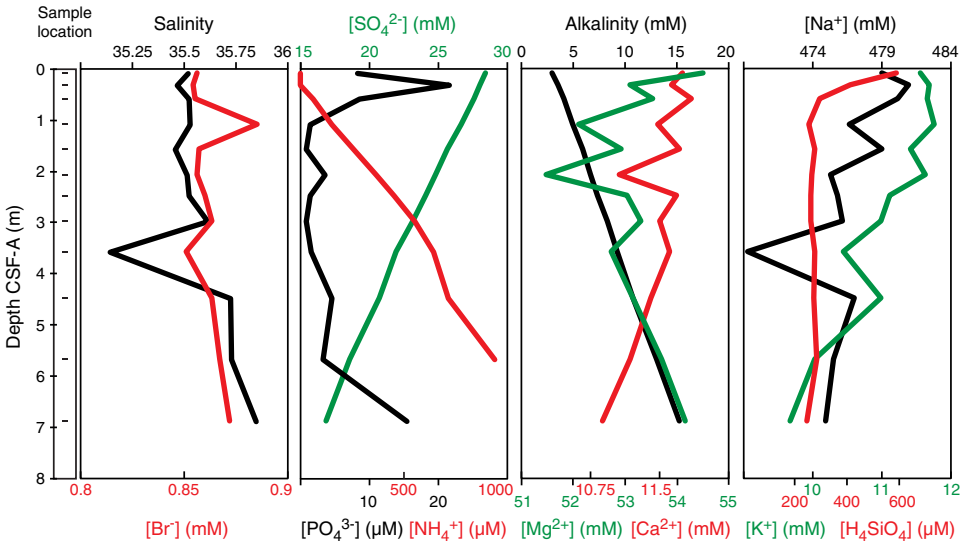

Table T12. TIC, $CaCO_3$, TC, and organic carbon contents, Site U1454. **Download table in .csv format.**

Figure F13. TIC content expressed as $CaCO_3$, Site U1454.

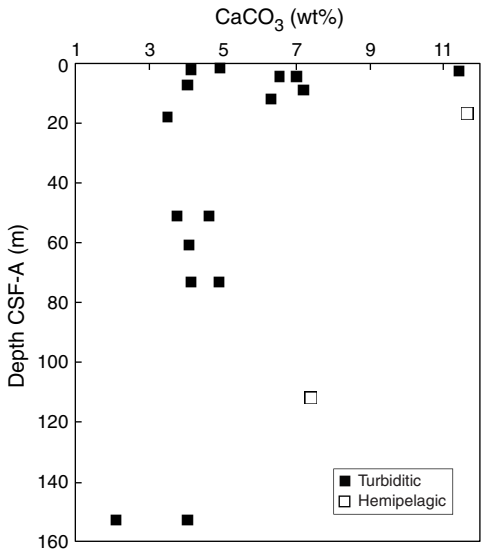

wt% were observed in the late glacial section of the levee of the active channel at 17°N (Lupker et al., 2013). In this levee, a systematic decrease in carbonate content across the deglaciation was inferred to reflect a change in weathering intensity. The carbonate content of turbiditic sediments from the active levee drilled at Site U1454 thus appears compatible with the composition of turbiditic sediments from the active levee at 17°N. The extreme paucity in turbiditic sediments with elevated carbonate content across the uppermost 200 m of the transect drilled at 8°N is conspicuous. This could reflect (1) unusual characteristics of the active levee and/or last glacial interglacial cycle deposits and/or (2) the overwhelming dominance of turbiditic sediments delivered and deposited during high-stand (i.e., interglacial-like) intervals in the Middle Bengal Fan.

Figure F14. TIC content expressed as $CaCO_3$ content of turbiditic sediments from Site U1454 (red squares) compared to $CaCO_3$ content of turbiditic sediments from the uppermost 200 m CSF-A of Sites U1449–U1453 and U1455 (black squares). The range in carbonate content of late glacial and Holocene turbiditic sediments from the levee of the active channel at 17°N is also shown for comparison (data from Lupker et al., 2013).

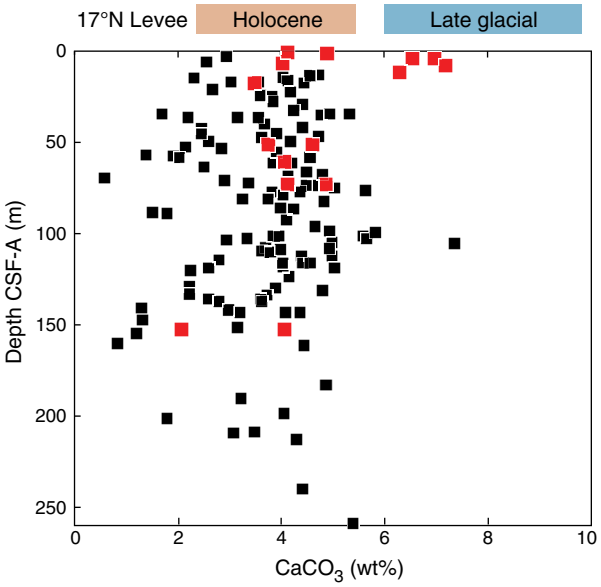

Organic carbon

Total carbon (TC) concentrations were determined on 18 sediment samples from Holes U1454A and U1454B (Table **T12**). TC values range from 0.4 to 2.1 wt%. Total organic carbon (TOC) content, calculated from the difference between TC and TIC, is low (average 0.5 wt%) and ranges between 0.1 and 0.8 wt% (Figure **F15**). In turbiditic sediments, TOC is variable and covaries with the Al/Si ratio (N = 10; not shown), reflecting the preferential association of organic matter with clays that has previously been documented in the modern Ganga-Brahmaputra river system, in active channel-levee sediments in the Bay of Bengal deposited over the past 18 ky (e.g.,

Galy et al., 2007), and in the uppermost 200 m cored at Sites U1449–U1453 and DSDP Site 218 (von der Borch, Sclater, et al., 1974).

ICP-AES results

Major and trace element concentrations were determined on 16 sediment samples from Holes U1454A and U1454B by inductively coupled plasma–atomic emission spectroscopy (ICP-AES) (Table **T13**). As at all previous sites, bulk-sediment major and trace element trends correspond closely with lithologic type. The Fe/Si or K/Si versus Al/Si trends for this data set (Figure **F16**) closely track those observed at Sites U1449–U1453 and in modern sediments in the Ganga-Brahmaputra river system (e.g., Lupker et al., 2012). In detail, the preliminary results from the active levee at 8°N do not show the K-depletion observed for the Holocene in the active levee at 17°N (Lupker et al., 2013). This implies that the material sampled here for ICP-AES analysis in the active levee at 8°N may be missing the last 11 ky and could suggest a different location for the active channel during at least some period of the Holocene. Alternatively, the transport mechanisms from the proximal to the middle part of the fan might be responsible for a change in the proportion of terrigeneous clays that carry the K-depletion signature.

Figure F15. TOC content, Site U1454.

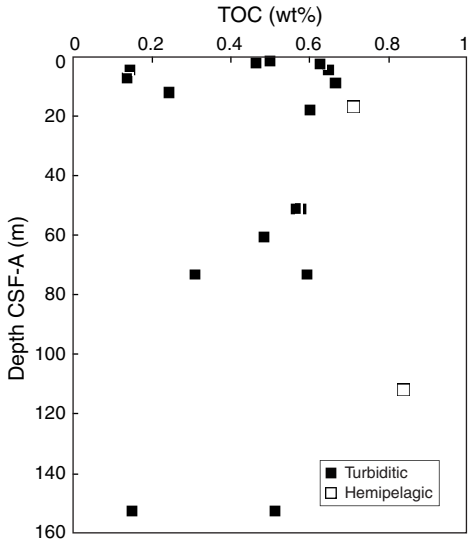

Table T13. Major elements and selected trace element contents, Site U1454.
Download table in .csv format.

Microbiology

A total of 20 microbiology whole-round core sections (12 from Hole U1454A and 8 from Hole U1454B) were collected on catwalk. The whole-round core sections were sampled for various microbiological investigations. A microbial cell counting method was initiated shipboard, with further processing of the samples to be performed following the expedition.

Figure F16. Fe/Si and K/Si vs. Al/Si, Site U1454.

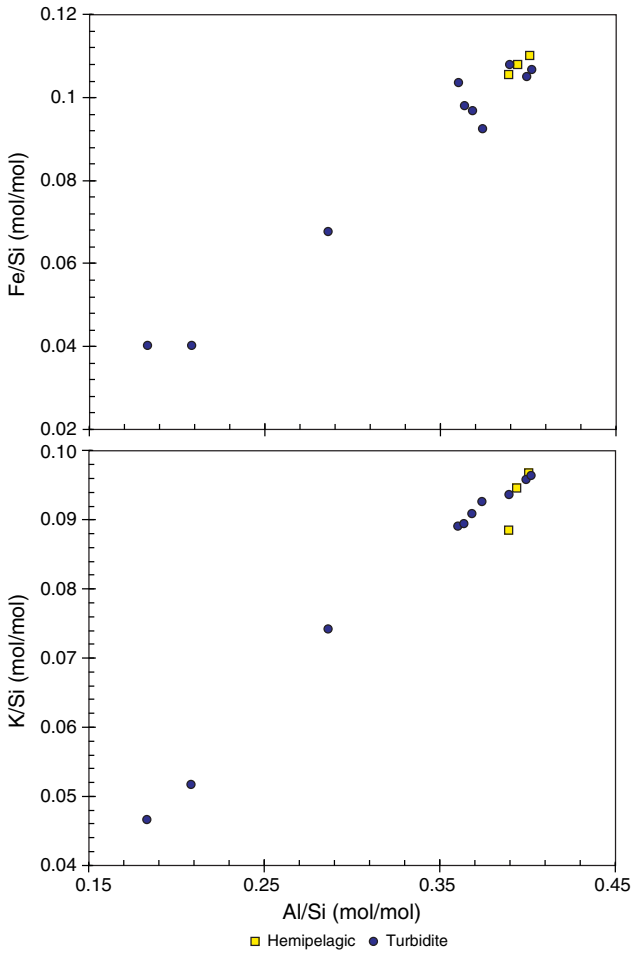

Physical properties

Physical property data were acquired in all Site U1454 holes, including density, magnetic susceptibility, *P*-wave velocity, NGR, and thermal conductivity (see **Physical properties** in the Expedition 354 methods chapter [France-Lanord et al., 2016a]). The site was cored with the APC and HLAPC systems to 161.8 CSF-A and recovered 127.7 m (79%) of sediment. Physical property data from Site U1454 are mostly of good quality (Figures **F17**, **F18**, **F19**) and reflect lithologic variations as at previous sites. Using the principal lithologic name from the core description to assign five lithologies (sand, silt, clay, calcareous clay, and volcanic ash; see **Lithostratigraphy**), we calculated their average physical properties (Table **T14**).

Accordingly, the most common principal lithology is sand (~56 m), followed by clay (~37 m), calcareous clay (~26 m), silt (~9 m), and volcanic ash occurring in minor proportions. Physical property measurements are described in detail below, but average values are as follows. Wet bulk densities are rather uniform for terrigenous sediment (sand, silt, and clay), ranging from 1.81 to 1.92 g/cm^3 on average. Volcanic ash has the lowest average wet bulk densities (1.67 g/cm^3), followed by calcareous clay (1.73 g/cm^3). Average *P*-wave velocities are highest in sand (1734 m/s on average) and lowest in clay (~1538 m/s) and calcareous clay (~1519 m/s). Average magnetic susceptibilities are also highest in sand (169 × 10^{-5} SI), followed by silt (104 × 10^{-5} SI) and clay (68 × 10^{-5} SI). The lowest values occur in calcareous clay (27 × 10^{-5} SI). NGR is high throughout the terrigenous components sand, silt, and clay (around 65–71 counts/s) and low in calcareous clay and volcanic ash (~52 counts/s). Thermal conductivity is highest in sand (1.90 W/[m·K]) and lowest in calcareous clay (1.15 W/[m·K]).

Figure F17. Physical property measurements, Site U1454.

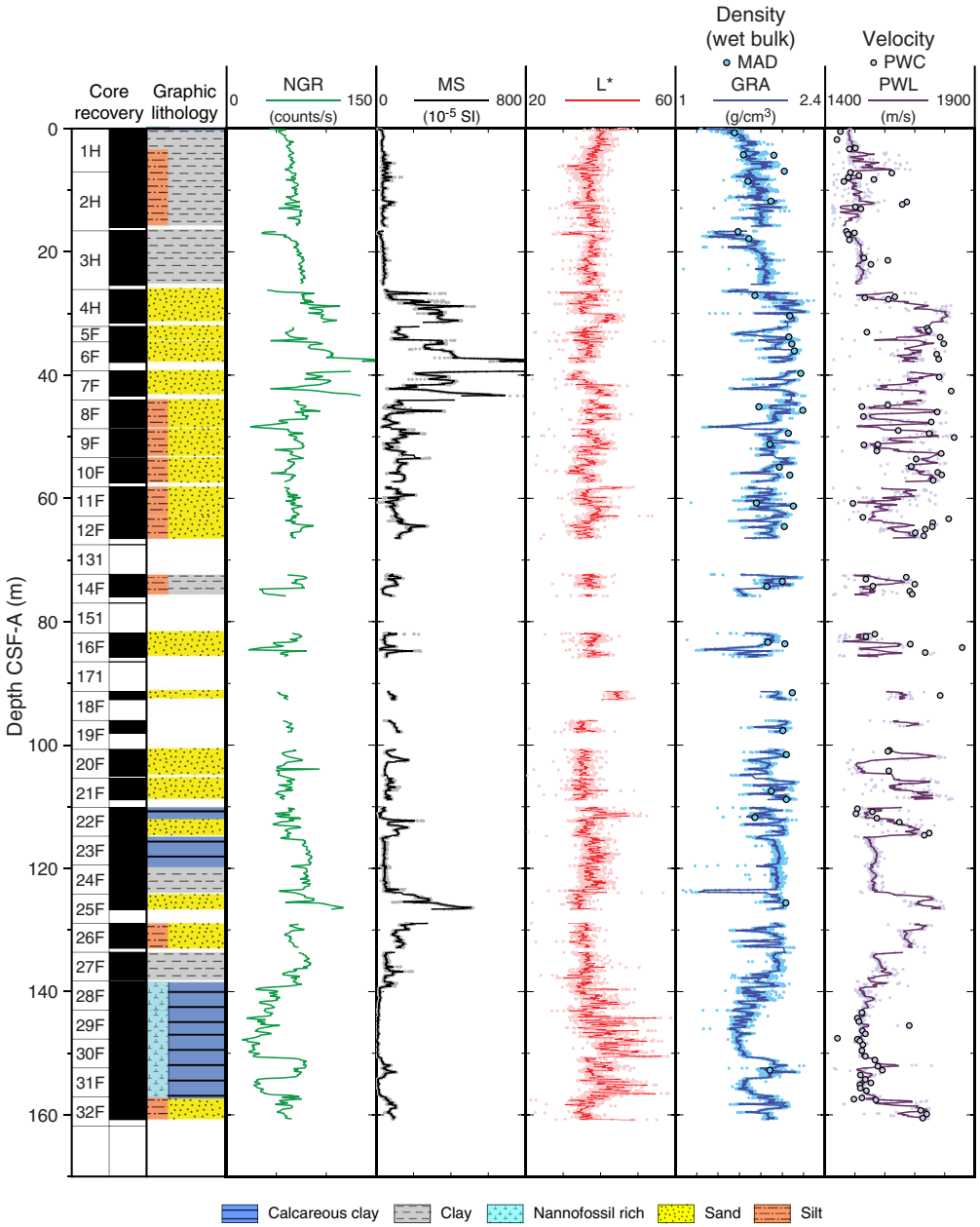

Figure F18. Moisture and density results, Hole U1454B.

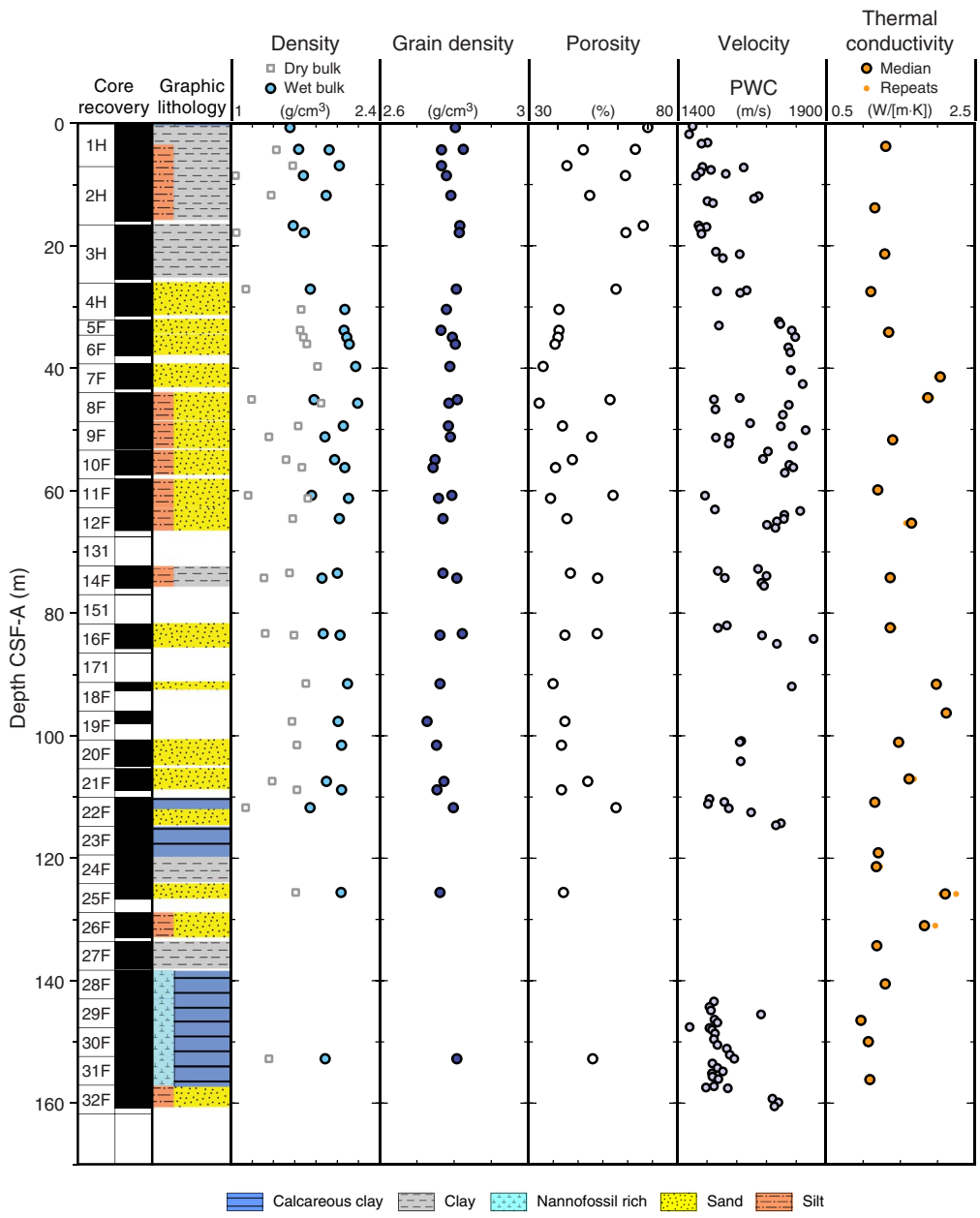

Physical property measurements and measurement intervals

High-resolution physical property measurements were made on Site U1454 cores to provide basic information on sediment composition and variability. Whole-Round Multisensor Logger (WRMSL) measurements were made at 1 cm increments for density by gamma ray attenuation (GRA), magnetic susceptibility, and compressional wave velocity on the *P*-wave logger (PWL). NGR measurements were made at 10 cm increments, and thermal conductivity measurements were made at one measurement per core.

On split cores, point magnetic susceptibility and color reflectance (RSC) were measured at 1 cm increments using the Section Half Multisensor Logger (SHMSL). Additionally, we took discrete samples for moisture and density (MAD) measurements (one or two samples per core, typically representing coarse-, medium-, and fine-grained intervals or pelagic intervals with varying carbonate or biogenic opal content) to determine water content, wet bulk density, dry bulk density, porosity, and grain density. *P*-wave velocity measurements were made on the half-core gantry caliper instrument (PWC) at one to three measurements per section where possible. The assignation into five different lithologies was taken from the core description (see **Lithostratigraphy**). Average physical properties for Site U1454 are given in Table **T14**.

Whole-Round Multisensor Logger measurements

Results from Site U1454 WRMSL measurements are compiled in Figure **F17**. For illustration purposes, data from the top and bottom 2 cm of each section were removed because they contain a cap

Figure F19. Physical property measurements, Cores 354-U1454B-26F through 32F. The interval at ~139–157 m CSF-A is a Middle Pleistocene hemipelagic unit (see **Paleomagnetism**) characterized by highs and lows in physical properties.

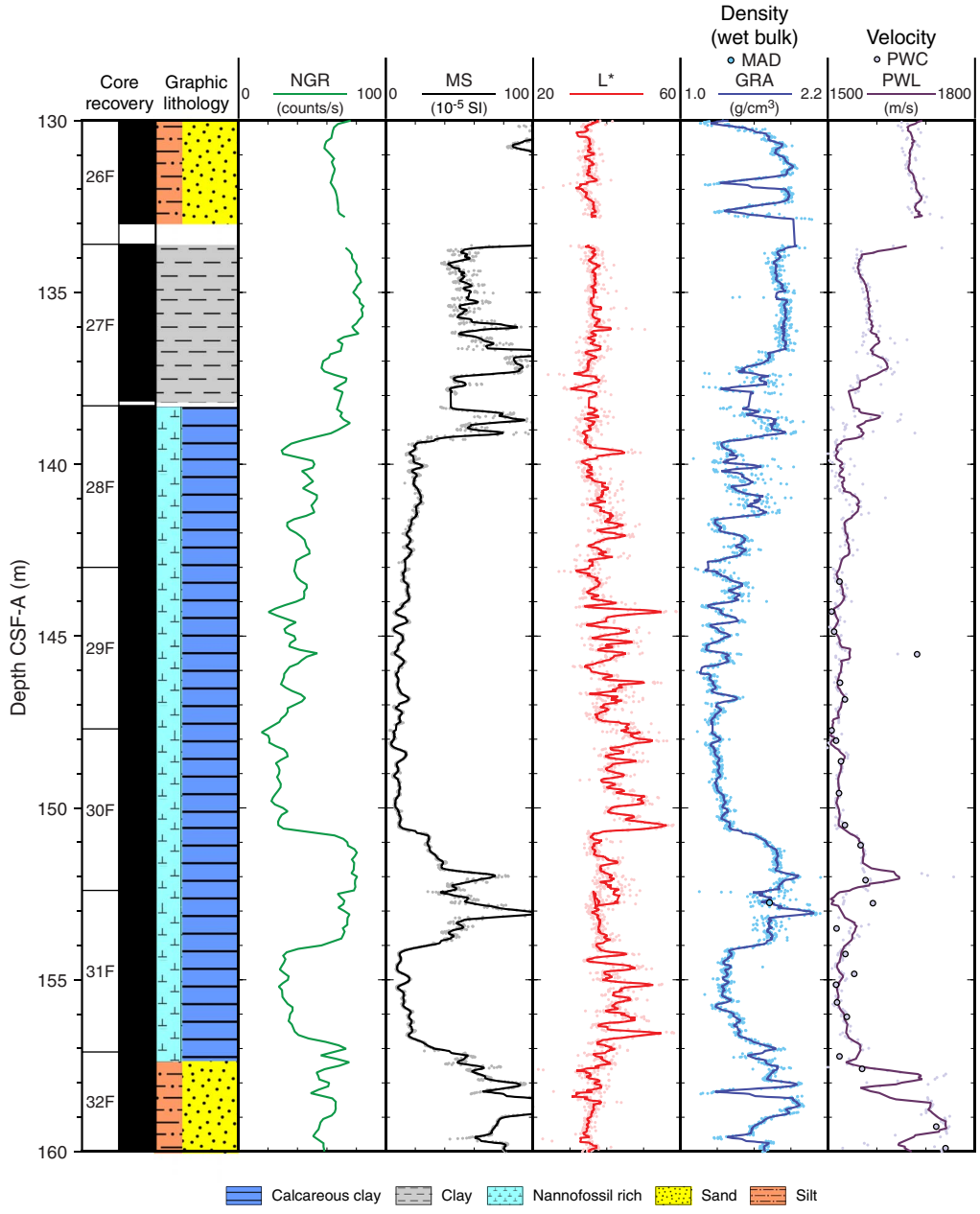

and often represent part sediment and part air and because the volume contributing to the measurement is unknown. Data that are unrealistic for the cored formations, such as densities <1.05 g/cm³ and velocities <1425 m/s or >3000 m/s, were also filtered out. All original data remain in the LIMS database.

Gamma ray attenuation bulk density

Average wet bulk densities (GRA) measured with the WRMSL range from 1.73 to 1.92 g/cm³, depending on lithology (Table **T14**). These values are in good agreement with MAD-determined wet bulk densities. Slightly higher MAD values were measured for sand. GRA values are lower in the uppermost, clayey Cores 354-U1454B-1H through 3H and in the lowermost, clayey to calcareous clayey Cores 27F–31F (Figure **F17**).

Magnetic susceptibility

Magnetic susceptibility is sensitive to the concentration and type of magnetic minerals. Average values are lowest in calcareous clay (27 × 10^{-5} SI), intermediate in clay (68 × 10^{-5} SI), and highest in sandy lithologies (169 × 10^{-5} SI; Table **T14**). These differences document again that the majority of lithologies can clearly be distinguished based on magnetic susceptibility measurements. Sandy Cores 6F–7F have the highest magnetic susceptibilities found during Expedition 354 (values in excess of 1000 × 10^{-5} SI; Figure **F17**). Values are also elevated in sandy Cores 25F–26F.

P-wave velocity

Average *P*-wave velocities from the PWL range from 1515 m/s for clay to 1657 m/s for sand (Table **T14**). PWL velocities are lower

Table T14. Total sediment thickness, percentage of recovered material, and average physical properties with respect to lithology, Site U1454. **Download table in .csv format.**

Site U1454 (161.8 m total penetration)	Sand	Silt	Clay	Calcareous clay	Volcanic ash	Total
Total thickness, m	55.83	8.93	36.76	25.58	0.07	127.17
Recovered material, %	43.90	7.00	28.90	20.10	0.10	79.00
Average GRA wet bulk density, g/cm^3	1.92	1.85	1.81	1.73	1.67	
Average MAD wet bulk density, g/cm^3	2.06	1.95	1.82	1.72		
Average MAD grain density, g/cm^3	2.77	2.78	2.80	2.81		
Average *P*-wave velocity (PWL), m/s	1657	1580	1515	1532	1593	
Average *P*-wave velocity (PWC), m/s	1734	1631	1538	1519	1682	
Average magnetic susceptibility (WRMSL), 10^{-5} SI	169	104	68	27	5	
Average magnetic susceptibility point (SHMSL), 10^{-5} SI	182	85	49	27	8	
Average natural gamma radiation (NGR), counts/s	70	65	72	52	53	
Average thermal conductivity, W/(m·K)	1.90	1.36	1.25	1.15		
Average reflectance L*	36.41	35.99	38.10	39.86	45.74	
Average reflectance a*	1.23	1.30	1.12	1.27	2.14	
Average reflectance b*	−2.54	−2.08	−2.08	−3.18	−2.34	

than PWC velocities. The discrepancy is large in sandy lithologies because of homogenized sands and lower in calcareous clay and clay. The PWL sensor was reconfigured for shorter stacking times, which allowed for routine measurements at 1 cm increments for this site. *P*-wave velocities are rather low in fine-grained cores rich in clay and calcareous clay (Cores 1H–3H and 27F–31F).

Natural gamma radiation

Average NGR values vary from 52 to 70 counts/s depending on lithology (Table **T14**). The lowest values are found in calcareous clay and volcanic ash, whereas the terrigenous lithologies sand, silt, and clay have commonly high values. NGR values display significant variations downcore (Figure **F17**), with minima in fine-grained sediment near the top (Cores 1H–3H) and base (Cores 28F–30F) of the site.

Thermal conductivity

Average thermal conductivities vary between 1.15 W/(m·K) for calcareous clay and 1.90 W/(m·K) for sandy lithologies (Table **T14**). Measurements were conducted with the needle probe. There is no obvious downcore trend documented by the data (Figure **F18**), but elevated values are mostly associated with sandy sections.

Point magnetic susceptibility

Point magnetic susceptibility measurements made with the SHMSL agree well with WRMSL susceptibility results for calcareous clay and volcanic ash. Average values are lower for silt and clay by ~15×10^{-5} to 20×10^{-5} SI, whereas sand displays higher values by ~15×10^{-5} SI (Table **T14**).

Discrete compressional wave velocity

Average PWC velocities for each principal lithology vary from 1518 to 1734 m/s, depending on lithology (Table **T14**). Average PWC velocities are higher than WRMSL velocities, with substantial differences in silt and sand (50–77 m/s) and volcanic ash (91 m/s).

Moisture and density

Water content, porosity, and wet and dry bulk densities are interdependent. Wet bulk densities determined with MAD procedures show less extreme variations than WRMSL measurements (Figures **F17**, **F18**). Average Site U1454 MAD wet bulk densities are highest for sand (~2.05 g/cm^3), followed by silt (~1.95 g/cm^3) and clay (1.86 g/cm^3), and are the lowest for calcareous clay 1.72 g/cm^3 (Table **T14**). Porosities range from 30% to 80%, depending on lithology. Average grain densities range from 2.77 to 2.81 g/cm^3.

Color reflectance

Average sediment lightness (L*) varies from ~36 to 38 for sand, silt, and clay, increasing to ~40 for calcareous clay and to 46 for volcanic ash (Table **T14**). L* values are generally lower in Cores 1H–14F, 4F–27F, 31F, and 32F. Higher values occur in Cores 16F–23F and 28F–31F.

Color component a*, the red–green component, shows rather similar averages of ~1.2 for all lithologies, except for volcanic ash, which averages ~2.1. Substantial variability is usually documented for calcareous clay. Color component b* is rather uniform in terrigenous lithologies, with average values around –2.3 and lower averages (bluer colors) for calcareous clay (–3.2). Values decrease downcore for the upper ~30 m.

Core disturbances and data quality

Core disturbances are displayed in Figure **F3**. They affect the quality and reliability of physical properties in various ways. For this APC- and HLAPC-cored hole, 127.17 m of recovery was relatively good (~79%), specifically for the upper and lower parts of Hole U1454B, although a significant portion of this was unconsolidated sand (56 m; 44%), for which some measurements are significantly affected.

Data variability and downhole trends

With only 161 m DSF total penetration depth, Site U1454 is one of the shorter sites cored during Expedition 354. Sediment recovered represents both fine-grained, muddy turbidites at the top and near the bottom of Hole U1454B, interbedded with mostly coarse-grained, sandy turbidites from Cores 4H–26F.

Cores 27F–31F recovered mostly pelagic sequences, generally termed calcareous clay (Figure **F19**). This ~18 m long interval corresponds to a Middle Pleistocene hemipelagic unit (~0.8 to ~1.2 Ma), which was repeatedly cored during Expedition 354 (see **Paleomagnetism**). This unit is clearly depicted by all physical properties, most prominently by decreased NGR, lower magnetic susceptibilities, higher and variable L* colors, lower wet bulk densities, and decreased *P*-wave velocities (Figure **F19**).

As at Sites U1449 and U1452, which have comparable lithologies, there is no clear downhole trend in physical properties. As at the previous sites, the physical properties obtained at Site U1454 correlate well with lithology and composition.

Downhole measurements

Downhole temperature and heat flow

One advanced piston corer temperature tool (APCT-3) downhole temperature measurement in Hole U1454B produced a value of 7.39°C at 152.4 m DSF (Figure **F20**), giving a geothermal gradient of about 39°C/km. The seafloor temperature was 1.5°C, based on APCT-3 data taken while the unit was held at the mudline for 5 min while lowering it into the hole.

Thermal conductivity under in situ conditions was estimated from laboratory-determined thermal conductivity from Hole U1454B using the method of Hyndman et al. (1974) (see **Physical properties** in the Expedition 354 methods chapter [France-Lanord et al., 2016a]). The calculated in situ values are within 2% of the measured laboratory values. Thermal resistance was then calculated by integrating the inverse of the in situ thermal conductivity over depth. A heat flow of 52 mW/m^2 was obtained from the linear fit between temperature and thermal resistance (Pribnow et al., 2000). The geothermal gradient and heat flow values at Site U1454 are within the normal range for ocean basins of same age of 90–100 Ma (Müller et al., 2008) and consistent with other measurements in the Bay of Bengal (Hasterok et al., 2011).

Stratigraphic synthesis

The main objective for Site U1454 drilling was to contribute to the reconstruction of the Pleistocene fan evolution as part of the seven-site drilling transect. Site U1454 is located ~600 m west of the inner flank of a channel system that had supposedly been active during the Holocene and thus represents the youngest channel-levee system drilled during Expedition 354. Bathymetry (Figure **F1**) reveals a pronounced meander loop eroding the western channel flank, with a point bar present on the opposite side, migrating northwestward. This location was added during the expedition as an alternate site to provide better age control on levee development and on terrigenous fluxes accumulating in the vicinity.

Seismic, physical properties, and lithology

Based on *Parasound* 4 kHz sediment echosounder data acquired during site surveys (Figure **F21**), the uppermost sedimentary unit at Site U1454 is distinctly different from most other sites of the Expedition 354 drilling transect. The ~5 m thick hemipelagic unit, marked by a strong reflection from the Toba ash horizon at other Expedition 354 sites, is absent, and instead, several units originating from levee sedimentation were identified. On top, a ~4 m thick low reflective layered levee unit is recognized, comprising the typical thickness decrease with increasing distance from the channel axis. Underlying this unit, a ~13 m thick levee unit with higher reflection amplitudes and more irregular reflectors is visible. This unit shows a less pronounced thickness decrease with increasing distance from the channel. Beneath it, a lower reflective unit is characterized by more continuous reflectors, also originating from levee sedimentation. Underneath the three levee units, echosounder data fail to resolve further details because of signal attenuation in coarse-grained sediments and irregular or rough interfaces.

Figure F20. APCT-3 temperature-time series, Hole U1454B.

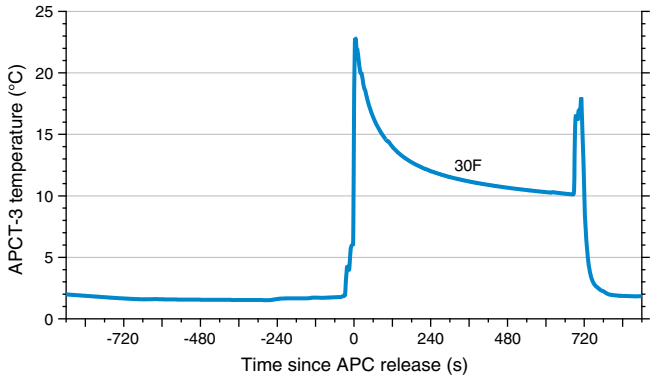

A comparison with the cored lithologies confirms the relationship between grain size and reflectivity on a much finer scale than the multichannel seismic data because a signal of 4 kHz main frequency, equivalent to ~40 cm wavelength, was emitted. The more reflective unit contains silt as a minor or major lithology with thicker silt beds, whereas the overlying and underlying units represent mud turbidites only, with minor proportions of silt. The downcore transition to sand is associated with higher signal scattering, as expected, and less clear imaging of interfaces.

An interval of calcareous clay that lacks silt beds and bioturbation was observed and identified at the top of Core 354-U1454B-3H, which may indicate reduced channel activity for a certain time period. The insert in Figure **F21** marks the thalweg, point bars (P), and likely migration direction of the point bar. Accordingly, channel sinuosity must have changed through time, leading to distinct phases of more silt-rich spillover sedimentation in between normal levee deposition (Schwenk et al., 2003). In multichannel seismic data (Figure **F22**) such fine details cannot be resolved. However, main lithologic changes are associated with changes in seismic facies, reflectivity, and reflector geometry and match very well. Also, contributions from nearby channels can be recognized by their seismic facies (e.g., at 5.07 or 5.17 s two-way traveltime [TWT]), and these can be correlated to turbiditic units in the lithology, which are intercalating the hemipelagic units toward the base of the hole.

Several hemipelagic units appear as low reflective bands of uniform thickness (e.g., at 5.11 and 5.15 s TWT). Seismic reflectors associated with these units (Figure **F22**; blue arrows) can be traced across the whole transect to Site U1451 and are useful stratigraphic markers.

Age-depth relationship

Because of the expanded Holocene and Pleistocene interval at this site, biostratigraphic constraints are limited. Three biomarkers (two nannofossil and one foraminiferal) were identified and are in agreement (Figure **F23**). Biostratigraphic refinement of this interval may be possible postexpedition by looking for additional Pleistocene nannofossil biohorizons, but this requires high-resolution sampling not feasible during the expedition.

The hemipelagic interval in lithostratigraphic Unit VI contains the Brunhes/Matuyama boundary (0.781 Ma), the lower Jaramillo geomagnetic reversal (1.072 Ma), and the short Matuyama-C1r-2r and Cobb Mountain (1.173–1.185 Ma) Subchrons (Figure **F23**). The Lower Jaramillo geomagnetic reversal was not recovered. It is most probably located in the gap between two cores. Sediment accumulation rates vary significantly in the hemipelagic and levee deposits

(Figure F24). They are ~1.4 cm/ky from ~1.2 to ~0.8 Ma in the hemipelagic layer. The sedimentation rate over the first 125 m of sediment calculated with the younger biostratigraphic tie point is ~43 cm/ky. However, this value is averaged over different types of sediment within the upper part of the section, where major changes in sedimentation rates are expected.

Achievements

Site U1454 provides a key expanded section to the overall understanding of depositional processes in the Pleistocene Bengal Fan. In addition to high-resolution nannofossil biostratigraphic work, the young—likely Holocene or late glacial—age of the channel will make it possible to date with oxygen isotopes and radiocarbon on foraminiferal tests as well as on terrestrial organic material. This was the main justification to add this site to the drilling transect during the expedition. Accordingly, we will be able to determine the time spans during which the identified levee units have formed. Also, the calcareous clay unit will shed light on the episodicity and absence of turbidites at this location. Furthermore, we expect to be able to link full channel activity with sea level and changes in terrestrial climate and to test the correlation between this levee record and the one already known at 16°30′N, which likely belongs to the same channel.

Beneath the levee, the cored section also consists of sand-rich units such as those at Site U1452, likely representing the progradational facies of early channel formation and erosion. Several other channel systems contributed to the accumulation, and it will be possible to constrain the temporal relationships between the various channel systems. Mud turbidites and silt and sand beds are intercalated between hemipelagic units, indicating strongly episodic activity, which may be correlated to sea level and climatic forcing.

This site also completes the westernmost recovery of the mid-Pleistocene hemipelagic interval along the 300 km transect. This will allow detailed investigations of the transition to intensified fan activity across the transect and, in comparison to Site U1455, reveal measures of distances over which the active channel can deliver fine particles and contribute to the dilution of hemipelagic accumulation.

Figure F21. *Parasound* sediment echosounder (4 kHz) Line SO125-GeoB97-020, Site U1454. For lithologic legend, see Figure F5 in the Expedition 354 methods chapter (France-Lanord et al., 2016a). Insert shows local bathymetry at the site; red dashed line = modern thalweg, black dashed arrow = migration of a point bar (P). Blue arrow = hemipelagic unit described in cores as calcareous clay. For a larger version of this figure, see STRATSYNTH in **Supplementary material**.

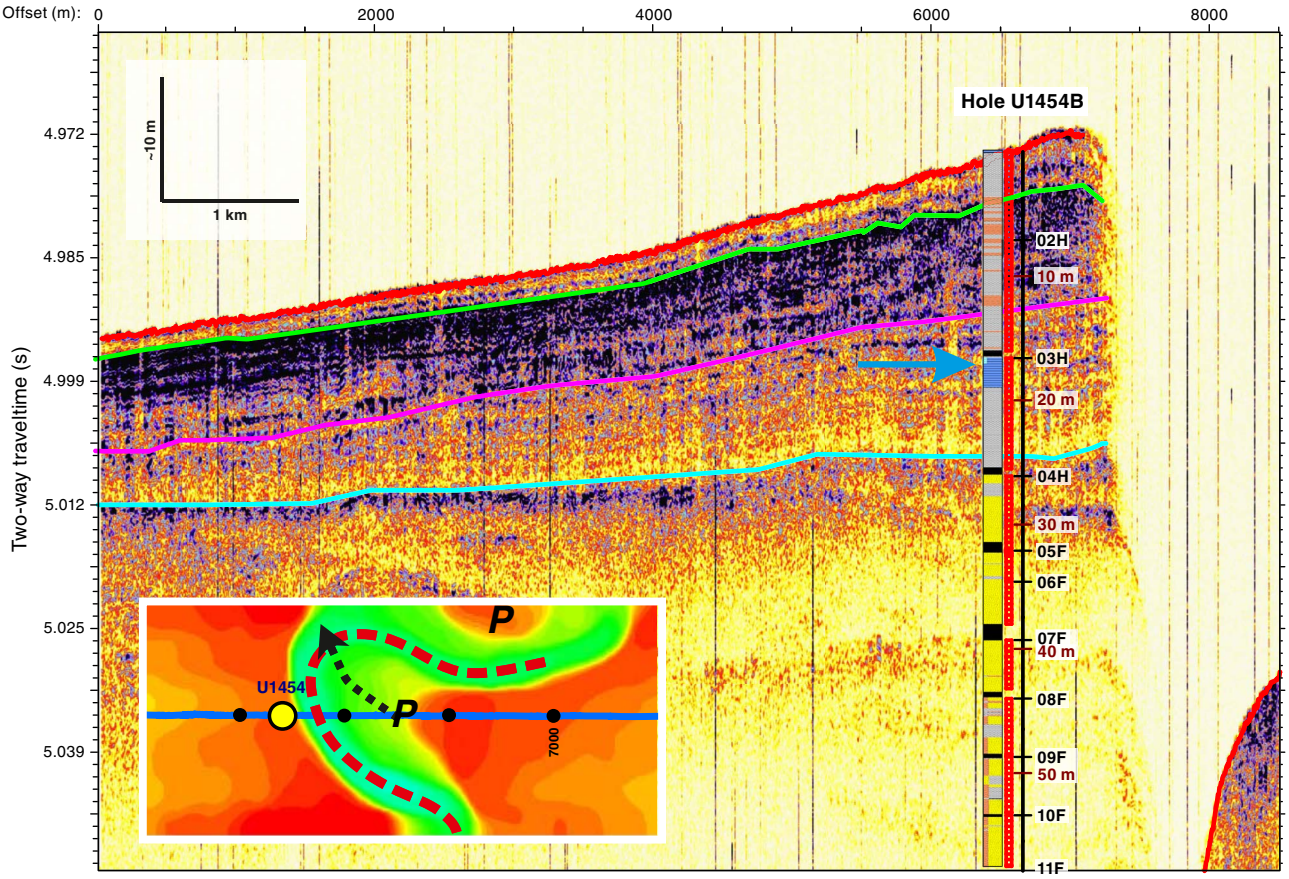

Figure F22. Seismic Line SO125-GeoB97-020, Site U1454. For lithologic legend, see Figure **F5** in the Expedition 354 methods chapter (France-Lanord et al., 2016a). Blue arrow = hemipelagic units described in cores as calcareous clay. For a larger version of this figure, see STRATSYNTH in **Supplementary material**.

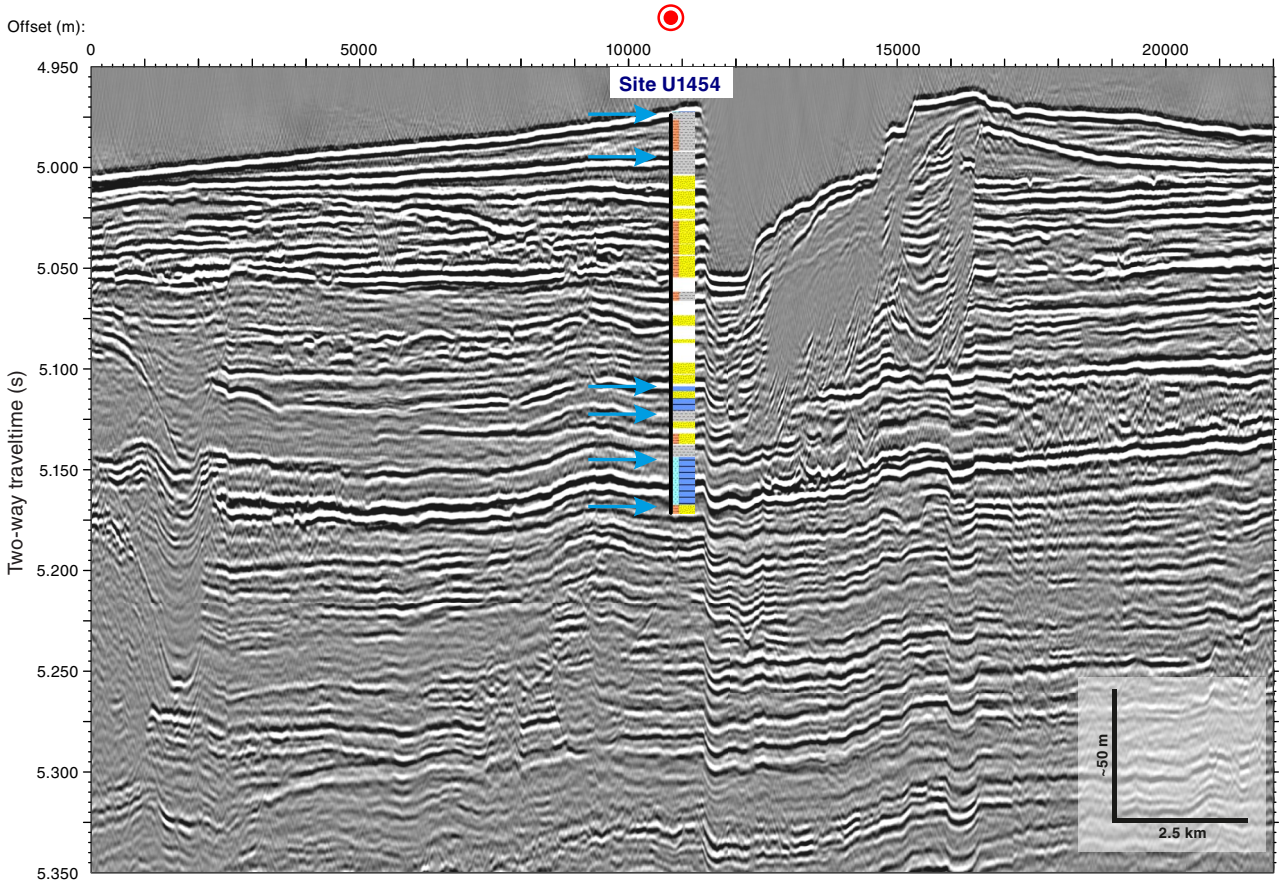

Figure F23. Compilation of biostratigraphic and chronostratigraphic markers, Site U1454. Calcareous nannofossil and foraminiferal biozones follow Gradstein et al. (2012; based on Martini [1971], Okada and Bukry [1980]) and Wade et al. (2011), respectively. Biomarkers are calculated as midpoints (Table **T6**). Paleomagnetic reversals follow the chronostratigraphic scheme of Gradstein et al. (2012); boundaries are the lower depth of the identified reversal (Table **T9**).

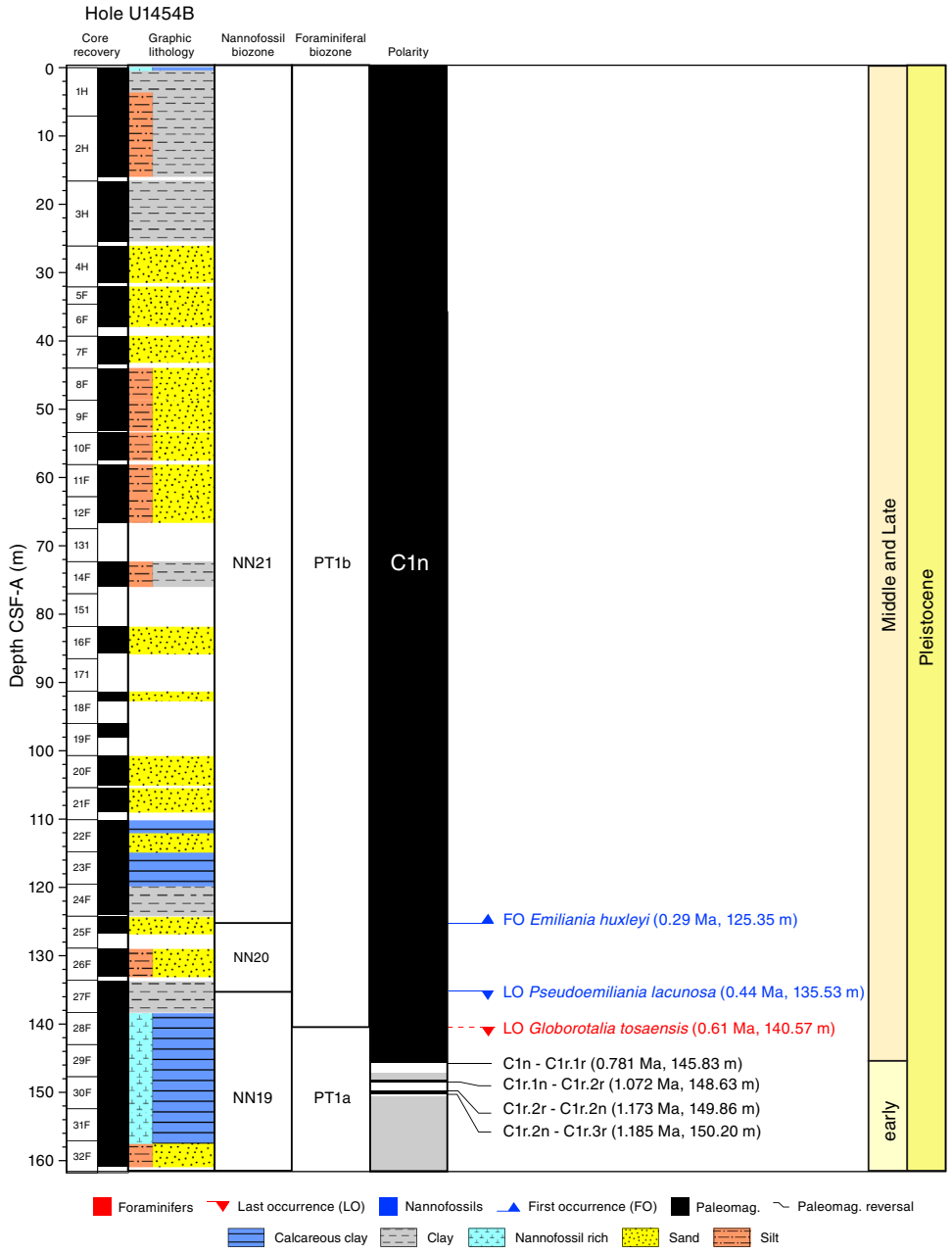

Figure F24. Age-depth plot, Hole U1454A. Interpreted lithology proposes the most probable lithologies in intervals of nonrecovery. Nannofossil and foraminiferal biomarkers are plotted as midpoints; error bars = uncertainty in depth. For biomarkers: right arrow = first occurrence, left arrow = last occurrence (Table **T6**). For magnetic reversals, see Table **T9**. Black arrows = selected accumulation rates. Dashed line = ash layer.

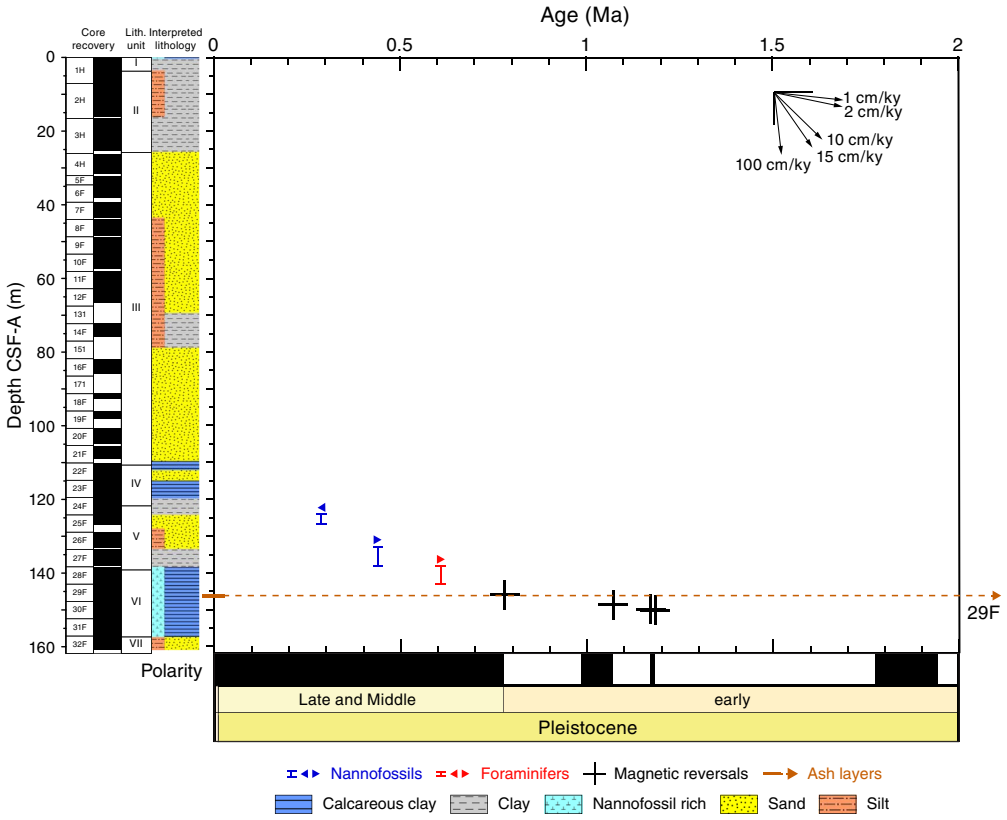

References

Bouquillon, A., France-Lanord, C., Michard, A., and Tiercelin, J.-J., 1990. Sedimentology and isotopic chemistry of the Bengal Fan sediments: the denudation of the Himalaya. *In* Cochran, J.R., Stow, D.A.V., et al., *Proceedings of the Ocean Drilling Program, Scientific Results,* 116: College Station, TX (Ocean Drilling Program), 43–58. **http://dx.doi.org/10.2973/odp.proc.sr.116.117.1990**

Chaisson, W.P., and Pearson, P.N., 1997. Planktonic foraminifer biostratigraphy at Site 925: middle Miocene–Pleistocene. *In* Shackleton, N.J., Curry, W.B., Richter, C., and Bralower, T.J. (Eds.), *Proceedings of the Ocean Drilling Program, Scientific Results,* 154: College Station, TX (Ocean Drilling Program), 3–31. **http://dx.doi.org/10.2973/odp.proc.sr.154.104.1997**

Curray, J.R., Emmel, F.J., and Moore, D.G., 2003. The Bengal Fan: morphology, geometry, stratigraphy, history and processes. *Marine and Petroleum Geology,* 19(10):1191–1223. **http://dx.doi.org/10.1016/S0264-8172(03)00035-7**

Dehn, J., Farrell, J.W., and Schmincke, H.-U., 1991. Neogene tephrochronology from Site 758 on northern Ninetyeast Ridge: Indonesian arc volcanism of the past 5 Ma. *In* Weissel, J., Peirce, J., Taylor, E., Alt, J., et al., *Proceedings of the Ocean Drilling Program, Scientific Results,* 121: College Station, TX (Ocean Drilling Program), 273–295. **http://dx.doi.org/10.2973/odp.proc.sr.121.123.1991**

France-Lanord, C., Spiess, V., Klaus, A., Adhikari, R.R., Adhikari, S.K., Bahk, J.-J., Baxter, A.T., Cruz, J.W., Das, S.K., Dekens, P., Duleba, W., Fox, L.R., Galy, A., Galy, V., Ge, J., Gleason, J.D., Gyawali, B.R., Huyghe, P., Jia, G., Lantzsch, H., Manoj, M.C., Martos Martin, Y., Meynadier, L., Najman, Y.M.R., Nakajima, A., Ponton, C., Reilly, B.T., Rogers, K.G., Savian, J.F., Schwenk, T., Selkin, P.A., Weber, M.E., Williams, T., and Yoshida, K., 2016a. Expedition 354 methods. *In* France-Lanord, C., Spiess, V., Klaus, A., Schwenk, T., and the Expedition 354 Scientists, *Bengal Fan*. Proceedings of the International Ocean Discovery Program, 354: College Station, TX (International Ocean Discovery Program). **http://dx.doi.org/10.14379/iodp.proc.354.102.2016**

France-Lanord, C., Spiess, V., Klaus, A., Adhikari, R.R., Adhikari, S.K., Bahk, J.-J., Baxter, A.T., Cruz, J.W., Das, S.K., Dekens, P., Duleba, W., Fox, L.R., Galy, A., Galy, V., Ge, J., Gleason, J.D., Gyawali, B.R., Huyghe, P., Jia, G., Lantzsch, H., Manoj, M.C., Martos Martin, Y., Meynadier, L., Najman, Y.M.R., Nakajima, A., Ponton, C., Reilly, B.T., Rogers, K.G., Savian, J.F., Schwenk, T., Selkin, P.A., Weber, M.E., Williams, T., and Yoshida, K., 2016b. Site U1451. *In* France-Lanord, C., Spiess, V., Klaus, A., Schwenk, T., and the Expedition 354 Scientists, *Bengal Fan*. Proceedings of the International Ocean Discovery Program, 354: College Station, TX (International Ocean Discovery Program). **http://dx.doi.org/10.14379/iodp.proc.354.105.2016**

France-Lanord, C., Spiess, V., Klaus, A., Adhikari, R.R., Adhikari, S.K., Bahk, J.-J., Baxter, A.T., Cruz, J.W., Das, S.K., Dekens, P., Duleba, W., Fox, L.R., Galy, A., Galy, V., Ge, J., Gleason, J.D., Gyawali, B.R., Huyghe, P., Jia, G., Lantzsch, H., Manoj, M.C., Martos Martin, Y., Meynadier, L., Najman, Y.M.R., Nakajima, A., Ponton, C., Reilly, B.T., Rogers, K.G., Savian, J.F., Schwenk, T., Selkin, P.A., Weber, M.E., Williams, T., and Yoshida, K., 2016c. Site U1452. *In* France-Lanord, C., Spiess, V., Klaus, A., Schwenk, T., and the Expedition 354 Scientists, *Bengal Fan*. Proceedings of the International Ocean Discovery Program, 354: College Station, TX (International Ocean Discovery Program). **http://dx.doi.org/10.14379/iodp.proc.354.106.2016**

France-Lanord, C., Spiess, V., Klaus, A., Schwenk, T., Adhikari, R.R., Adhikari, S.K., Bahk, J.-J., Baxter, A.T., Cruz, J.W., Das, S.K., Dekens, P., Duleba, W., Fox, L.R., Galy, A., Galy, V., Ge, J., Gleason, J.D., Gyawali, B.R., Huyghe, P., Jia, G., Lantzsch, H., Manoj, M.C., Martos Martin, Y., Meynadier, L., Najman, Y.M.R., Nakajima, A., Ponton, C., Reilly, B.T., Rogers, K.G., Sav-

ian, J.F., Selkin, P.A., Weber, M.E., Williams, T., and Yoshida, K., 2016d. Expedition 354 summary. *In* France-Lanord, C., Spiess, V., Klaus, A., Schwenk, T., and the Expedition 354 Scientists, *Bengal Fan*. Proceedings of the International Ocean Discovery Program, 354: College Station, TX (International Ocean Discovery Program). **http://dx.doi.org/10.14379/iodp.proc.354.101.2015**

Galy, V., France-Lanord, C., Beyssac, O., Faure, P., Kudrass, H., and Palhol, F., 2007. Efficient organic carbon burial in the Bengal Fan sustained by the Himalayan erosional system. *Nature,* 450(7168):407–410. **http://dx.doi.org/10.1038/nature06273**

Galy, V., François, L., France-Lanord, C., Faure, P., Kudrass, H., Palhol, F., and Singh, S.K., 2008. C4 plants decline in the Himalayan basin since the Last Glacial Maximum. *Quaternary Science Reviews,* 27(13–14):1396–1409. **http://dx.doi.org/10.1016/j.quascirev.2008.04.005**

Garzanti, E., Vezzoli, G., Andò, S., France-Lanord, C., Singh, S.K., and Foster, G., 2004. Sand petrology and focused erosion in collision orogens: the Brahmaputra case. *Earth and Planetary Science Letters,* 220(1–2):157–174. **http://dx.doi.org/10.1016/S0012-821X(04)00035-4**

Gradstein, F.M., Ogg, J.G., Schmitz, M.D., and Ogg, G.M. (Eds.), 2012. *The Geological Time Scale 2012:* Amsterdam (Elsevier).

Hasterok, D., Chapman, D.S., and Davis, E.E., 2011. Oceanic heat flow: implications for global heat loss. *Earth and Planetary Science Letters,* 311(3–4):386–395. **http://dx.doi.org/10.1016/j.epsl.2011.09.044**

Hübscher, C., Spieß, V., Breitzke, M., and Weber, M.E., 1997. The youngest channel-levee system of the Bengal Fan: results from digital sediment echosounder data. *Marine Geology,* 141(1–4):125–145. **http://dx.doi.org/10.1016/S0025-3227(97)00066-2**

Hyndman, R.D., Erickson, A.J., and Von Herzen, R.P., 1974. Geothermal measurements on DSDP Leg 26. *In* Davies, T.A., Luyendyk, B.P., et al., *Initial Reports of the Deep Sea Drilling Project,* 26: Washington, DC (U.S. Government Printing Office), 451–463. **http://dx.doi.org/10.2973/dsdp.proc.26.113.1974**

Lupker, M., France-Lanord, C., Galy, V., Lavé, J., Gaillardet, J., Gajurel, A.P., Guilmette, C., Rahman, M., Singh, S.K., and Sinha, R., 2012. Predominant floodplain over mountain weathering of Himalayan sediments (Ganga basin). *Geochimica et Cosmochimica Acta,* 84:410–432. **http://dx.doi.org/10.1016/j.gca.2012.02.001**

Lupker, M., France-Lanord, C., Galy, V., Lavé, J., and Kudrass, H., 2013. Increasing chemical weathering in the Himalayan system since the Last Glacial Maximum. *Earth and Planetary Science Letters,* 365:243–252. **http://dx.doi.org/10.1016/j.epsl.2013.01.038**

Martini, E., 1971. Standard Tertiary and Quaternary calcareous nannoplankton zonation. *In* Farinacci, A. (Ed.), *Proceedings of the Second Planktonic Conference, Roma 1970:* Rome (Edizioni Tecnoscienza), 2:739–785.

Müller, R.D., Sdrolias, M., Gaina, C., and Roest, W.R., 2008. Age, spreading rates, and spreading asymmetry of the world's ocean crust. *Geochemistry, Geophysics., Geosystems,* 9(4):Q04006. **http://dx.doi.org/10.1029/2007GC001743**

Okada, H., and Bukry, D., 1980. Supplementary modification and introduction of code numbers to the low-latitude coccolith biostratigraphic zonation (Bukry, 1973; 1975). *Marine Micropaleontology,* 5:321–325. **http://dx.doi.org/10.1016/0377-8398(80)90016-X**

Pribnow, D., Kinoshita, M., and Stein, C., 2000. *Thermal Data Collection and Heat Flow Recalculations for Ocean Drilling Program Legs 101–180*: Hanover, Germany (Institute for Joint Geoscientific Research, Institut für Geowissenschaftliche Gemeinschaftsaufgaben [GGA]). **http://www-odp.tamu.edu/publications/heatflow/ODPReprt.pdf**

Schwenk, T., Spieß, V., Hübscher, C., and Breitzke, M., 2003. Frequent channel avulsions within the active channel–levee system of the middle Bengal Fan—an exceptional channel–levee development derived from parasound and hydrosweep data. *Deep Sea Research, Part II: Topical Studies in Oceanography,* 50(5):1023–1045. **http://dx.doi.org/10.1016/S0967-0645(02)00618-5**

von der Borch, C.C., Sclater, J.G., et al., 1974. *Initial Reports of the Deep Sea Drilling Project,* 22: Washington (U.S. Government Printing Office). **http://dx.doi.org/10.2973/dsdp.proc.22.1974**

Wade, B.S., Pearson, P.N., Berggren, W.A., and Pälike, H., 2011. Review and revision of Cenozoic tropical planktonic foraminiferal biostratigraphy and calibration to the geomagnetic polarity and astronomical time scale. *Earth-Science Reviews,* 104(1–3):111–142. **http://dx.doi.org/10.1016/j.earscirev.2010.09.003**

Weber, M.E., Wiedicke, M.H., Kudrass, H.R., Hübscher, C., and Erlenkeuser, H., 1997. Active growth of the Bengal Fan during sea-level rise and highstand. *Geology,* 25(4):315–318. **http://dx.doi.org/10.1130/0091-7613(1997)025<0315:AGOTBF>2.3.CO;2**